**ATLAS Note**

# Search for flavor-changing neutral currents $tHq$ interactions with $H \rightarrow \tau^+\tau^-$ in proton-proton collisions at $\sqrt{s} = 13$ TeV

The ATLAS Collaboration

5th August 2020

A search is presented for flavor-changing neutral currents $tHq$ interactions with $H \rightarrow \tau^+\tau^-$ using a data set collected with the ATLAS detector at the LHC, corresponding to an integrated luminosity of 140 fb$^{-1}$ of proton-proton collisions at a center-of-mass energy of 13 TeV. The search is performed in the decay chain $t\bar{t} \rightarrow Wb + Hq$ or $qg \rightarrow tH \rightarrow Wb + H$ ($q = c/u$), where the $W$ boson decays inclusively and H decays to $\tau^+\tau^-$. Upper limits at 95 % confidence level for the coupling coefficient are measured to be $XXX$ and $XXX$, while the expected limits are $XXX^{+XXX}_{-XXX}$% and $XXX^{+XXX}_{-XXX}$%, respectively.

To be done:

1) Theory systematics

2) Systematics for lepton channels

# Contents

# Contents

# 1 Introduction

## 2 Introduction

Since the discovery of the Higgs boson in 2012, great efforts are made to study its properties. As the mass of the Higgs boson is about 125 GeV [**HiggsMass**], it is kinematically allowed that a top quark decays to a Higgs boson and an up-type quark via the flavour-changing neutral current (FCNC). In the Standard Model (SM), the FCNC interaction is forbidden at tree level and suppressed at higher orders due to the Glashow-Iliopoulos-Maiani (GIM) mechanism [**GIM**]. The $t \rightarrow u/c + H$ branching fraction in the SM is calculated to be around $10^{-15}$ [**brtch3**]. It would be enhanced in many models beyond the SM (BSM). Examples are the quark-singlet model [**quarkSinglet1**, **quarkSinglet2**], the two-Higgs doublet model with or without the flavour violation [**2hdm1**, **2hdm2**], the minimal supersymmetric standard model (MSSM) [**2hdm3**], supersymmetry with R-parity violation [**Rparity**], the Topcolour-assisted Technicolour model [**Techni**] or models with warped extra dimensions [**extraD**], the little Higgs model with T-parity conservation [**littleH**] and the composite Higgs models [**compositeH**]. Especially, the ansatz of Cheng and Sher [**Sher**] allows a branching fraction of about $10^{-3}$ [**FCNC_rate**]. Therefore, an observation of this decay would be a clear evidence for new physics.

On the other hand, if the $tHq$ interaction exists, the single-top, Higgs associated production through this interaction should also be enhanced. The $tH$ associated production in the SM prediction is expected to be small at LHC[**tHjb_production**]. So the study on this process will also contribute to the FCNC interaction searches.

Upper 95% CL limits on BR($t \rightarrow Hq$) have been obtained by ATLAS based on the data from 2015 and 2016, in the $H \rightarrow \gamma\gamma$ [**fcncgmgm**], $H \rightarrow WW/\tau_{\text{lep}}\tau_{\text{lep}}$ multilepton [**fcncml**] and $H \rightarrow \tau\tau$, $H \rightarrow b\bar{b}$ [**fcnctautau**] channels. The combined expected (observed) limits are 0.083% (0.11%) and 0.083% (0.12%) for $t \rightarrow Hc$ and $t \rightarrow Hu$, respectively.

The $t \rightarrow Hq$ decay and $gq \rightarrow tH$ production are also searched by CMS based on the data from 2015 and 2016[**CMS-TOP-17-003**].

The FCNC coupling is parametrised using dim-6 operators [**fcnc_production_theory**]. The effective Lagrangian regarding $tqH$ interaction before spontaneously symmetry breaking is:

$$\mathcal{L}_{EFT} = \frac{C_{u\phi}^{i3}}{\Lambda^2}(\phi^\dagger\phi)(\bar{q}_i t)\tilde{\phi} + \frac{C_{u\phi}^{3i}}{\Lambda^2}(\phi^\dagger\phi)(\bar{Q}u_i)\tilde{\phi} + H.c \tag{1}$$

Where the the operator notation is consistent with [**fcnc_production_theory**]. $C^{i3}$ is the Wilson coefficient of the 6-dim operator with $i = 1, 2$ denoting the flavor of upper type quark. $\Lambda$ is the scale of the new physics where the UV cut off happens which is set as 1 TeV as benchmark. $\phi$ is the SM higgs doublet. $\tilde{\phi} = \epsilon\phi^*$ where $\epsilon$ is the antisymmetric matrix with $\epsilon_{12} = -\epsilon_{21} = 1$.

The Wilson coefficient $C_{u\phi}$'s can be extracted as

$$(C_{u\phi}^{i3})^2 + (C_{u\phi}^{3i})^2 = 1946.6 \, \text{BR}(t \to qH)$$
$$(C_{u\phi}^{13})^2 + (C_{u\phi}^{31})^2 = \sigma(ug \to tH)/365.2 \, \text{fb} \tag{2}$$
$$(C_{u\phi}^{23})^2 + (C_{u\phi}^{32})^2 = \sigma(cg \to tH)/52.9 \, \text{fb}$$

To give a better impression on the numbers, we use $\text{BR}(t \to qH) = 1(0.2)\%$ as benchmark, which is corresponding to $(C_{u\phi}^{13})^2 + (C_{u\phi}^{31})^2 = 19.47(3.89)$, $\sigma(ug \to tH) = 7109.0(1421.8)$ pb, $\sigma(cg \to tH) = 1029.8(206.0)$ pb.

In this article, a search for the decay $t \to qH$ in the $t\bar{t}$ production (TT) and single-top, Higgs associated production (ST) with $H \to \tau\tau$ as shown in Fig 1 using 140 fb$^{-1}$ of proton-proton collision data at 13 TeV, taken with the ATLAS detector at the Large Hadron Collider (LHC), is presented. The final state is characterized by one top and one Higgs. In TT, there is an additional u/c quark forming a top resonance with Higgs.
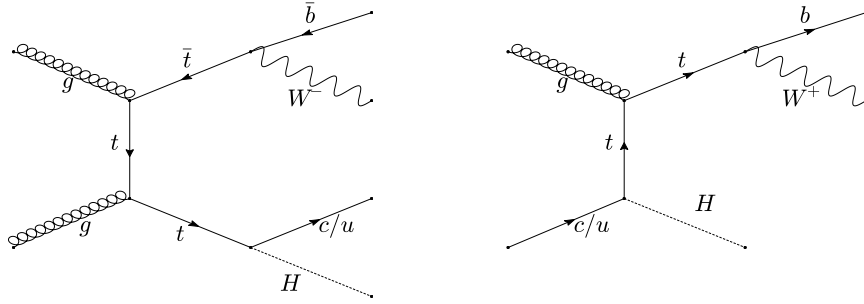


Figure 1: Diagrams of FCNC TT(left) and ST(right) process.

# 3 Detector, data set and Monte Carlo simulation

## 3.1 ATLAS detector

The ATLAS detector [PERF-2007-01] at the LHC covers nearly the entire solid angle around the collision point. It consists of an inner tracking detector surrounded by a thin superconducting solenoid, electromagnetic and hadronic calorimeters, and a muon spectrometer incorporating three large superconducting toroid magnets.

The inner-detector system (ID) is immersed in a 2 T axial magnetic field and provides charged particle tracking in the range $|\eta| < 2.5$. A high-granularity silicon pixel detector covers the vertex region and typically provides three measurements per track. It is followed by a silicon microstrip tracker, which usually

105 provides four two-dimensional measurement points per track. These silicon detectors are complemented
106 by a transition radiation tracker, which enables radially extended track reconstruction up to $|\eta| < 2.0$.
107 The transition radiation tracker also provides electron identification information based on the fraction of
108 hits above a higher energy-deposit threshold corresponding to transition radiation. Compared to Run-1,
109 an Insertable B-Layer [**IBL**] (IBL) is inserted as the innermost pixel layer during LS1 for Run-2, which
110 significantly improves the tracking performance.

111 The calorimeter system covers the pseudorapidity range $|\eta| < 4.9$. Within the region $|\eta| < 3.2$, electromag-
112 netic calorimetry is provided by barrel and endcap high-granularity liquid-argon (LAr) electromagnetic
113 calorimeters, with an additional thin LAr presampler covering $|\eta| < 1.8$, to correct for energy loss in
114 material upstream of the calorimeters. Hadronic calorimetry is provided by a scintillator-tile calorimeter,
115 segmented into three barrel structures within $|\eta| < 1.7$, and two LAr hadronic endcap calorimeters.

116 A muon spectrometer (MS) comprises separate trigger and high-precision tracking chambers measuring
117 the deflection of muons in a magnetic field generated by superconducting air-core toroids. The precision
118 chamber system covers the region $|\eta| < 2.7$ with three layers of monitored drift tubes, complemented by
119 cathode strip chambers in the forward region, where the background is highest. The muon trigger system
120 covers the range $|\eta| < 2.4$ with resistive-plate chambers in the barrel, and thin-gap chambers in the endcap
121 regions.

## 3.2  Data set

123 This analysis is based on the full proton-proton data at a center-of-mass energy $\sqrt{s} = 13$ TeV with a bunch
124 spacing of 25 ns collected by ATLAS in Run-2. The following good run list (GRL) was used for the 2015
125 dataset:

126 data15_13TeV.periodAllYear_DetStatus-v89-pro21-02_Unknown_PHYS_StandardGRL_All_Good_25ns.xml

127 which corresponds to an integrated luminosity of 3.22 fb$^{-1}$.

128 The GRL used for the 2016 dataset:

129 data16_13TeV.periodAllYear_DetStatus-v89-pro21-01_DQDefects-00-02-04_PHYS_StandardGRL_All_Good_25ns.x

130 corresponds to an integrated luminosity of 32.88 fb$^{-1}$.

131 These GRLs exclude data where the IBL was not fully operational. The uncertainty in the combined
132 2015+2016 integrated luminosity, 36.1 fb$^{-1}$, is 2.1%. It is derived, following a methodology similar to
133 that detailed in Ref. [**DAPR-2013-01**], from a calibration of the luminosity scale using x-y beam-separation
134 scans performed in August 2015 and May 2016.

135 The GRL used for the 2017 dataset:

136  data17_13TeV.periodAllYear_DetStatus-v99-pro22-01_Unknown_PHYS_StandardGRL_All_Good_25ns_Triggerno17

137  corresponds to an integrated luminosity of 44.307 fb$^{-1}$.

138  The GRL used for the 2018 dataset:

139  data18_13TeV.periodAllYear_DetStatus-v102-pro22-04_Unknown_PHYS_StandardGRL_All_Good_25ns_Triggerno1

140  corresponds to an integrated luminosity of 59.937 fb$^{-1}$. The final luminosity used for the analysis is

141  140.45 fb$^{-1}$.

## 3.3  Signal and background simulation

143  The overview of the major samples generated is summarized in table 1.

144  The TopFCNC UFO model [**FCNC_UFO1**, **FCNC_UFO2**] with 5-flavour scheme is used for signal
145  simulation.

146  The FCNC ST signal is simulated using MadGraph5_aMC@NLO v2.6.2 [**MG5**] interfaced with Pythia
147  8 [**Pythia8**] with the A14 tune [**A14**] for the generation of parton showers, hadronisation and multiple
148  interactions and the NNPDF30NLO [**NNPDF30NLO**] parton distribution functions (PDF) is used to
149  generate $qg$ events at next-to-leading order (NLO) in QCD. Depending on either up quark or charm quark
150  involved in the FCNC decay and either the $W$ bosons decaying hadronically or leptonically, 4 samples are
151  generated for each term of effective Lagrangian, so eight samples in total.

152  The FCNC TT signal is simulated using Powheg-Box [**Powheg**] V2 interfaced with Pythia8 [**Pythia8**]
153  with the A14 tune [**A14**] for the generation of parton showers, hadronisation and multiple interactions and
154  the NNPDF30NLO [**NNPDF30NLO**] parton distribution functions (PDF) is used to generate $t\bar{t}$ events at
155  next-to-leading order (NLO) in QCD. Depending on either the top or the anti-top quark decaying to $bW$,
156  either up quark or charm quark involved in the FCNC decay and either the $W$ bosons decaying hadronically
157  or leptonically, eight samples are produced with the Higgs going to a $\tau$-lepton pair.

158  The dominant background is the $t\bar{t}$ production. The $t\bar{t}$ process and the single top process are generated with
159  Powheg-Box [**Powheg**] V2, and Pythia8 is used for the parton shower. NNPDF30NLO [**NNPDF30NLO**]
160  and A14 tune [**A14**] are used for $t\bar{t}$(single top). The $t\bar{t}$ sample is also generated with different generators
161  and parton showers models, as well as different amount of radiations, for systematics as detailed in Sec.
162  10.

163  The $t\bar{t}X$, where X=$W$, $ee$, $\mu\mu$, $\tau\tau$ or $Z(qq, \nu\nu)$ ($\tau\tau$ has the Higgs resonance excluded), are generated
164  with MadGraph5_aMC@NLO and inferfaced with Pythia8 for the parton shower. The NNPDF30NLO
165  [**NNPDF30NLO**] is used for the matrix element PDF. The $t\bar{t}$, single top and $t\bar{t}X$ are combined into a
166  single process named top background in the analysis.

Table 1: Overview of the MC generators used for the main signal and background samples

| Process | Generator | | PDF set | | Tune | Order |
|---|---|---|---|---|---|---|
| | ME | PS | ME | PS | | |
| TT Signal | Powheg | Pythia8 | NNPDF30NLO | NNPDF23LO | A14 | NLO |
| ST Signal | MadGraph5_aMC@NLO | Pythia8 | NNPDF30NLO | NNPDF23LO | A14 | NLO |
| $W/Z$+jets | Sherpa 2.2.1 | | NNPDF30NNLO | | Sherpa | NLO/LO |
| $t\bar{t}$ | Powheg | Pythia8 | NNPDF30NLO | NNPDF23LO | A14 | NLO |
| Single top | Powheg | Pythia6 | CT10(NLO) | CTEQ6L1[**CTEQ**] | Perugia2012 | NLO |
| $t\bar{t}X$ | MadGraph5_aMC@NLO | Pythia8 | NNPDF30NLO | NNPDF23LO | A14 | NLO |
| Diboson | Sherpa 2.2.1 | | NNPDF30NNLO | | Sherpa | NLO/LO |

The $W$+jets, $Z$+jets and diboson backgrounds are simulated using Sherpa 2.2.1 [**Sherpa**] with NNPDF30NNLO PDF [**NNPDF30NLO**].

The $\tau$ decay in the single top samples is handled by Tauola [**Tauola**]. All samples showered by Pythia8 (Sherpa) have the $\tau$ decays also handled by Pythia8 (Sherpa). All the decay modes of the $\tau$ lepton are allowed in the event generators (but may be subject to generator filters). The summary of used generators for matrix element and parton shower is given in Tab. 1.

The SM higgs background includes $ggH$, $VH$, $VBF$ and $t\bar{t}H$, generated from Powheg-Box [**Powheg**] V2 interfaced with Pythia8. The overall contribution is pretty small. Various PDF and tune options are use for those samples depending on the decay modes.

The $tH$ associated production is negligible but we still considered it. The sample is generated using MadGraph5 and interfaced with pythia8 for parton shower. CT10 PDF and A14 tune are used. It is treated as part of SM higgs background explained in above.

All Monte-Carlo (MC) samples were passed through the full GEANT4 [**GEANT4**] simulation of the ATLAS detector, except for two extra $t\bar{t}$ samples with Pythia8 and Herwig7 [**Herwig**] parton showering which are simulated with ATLFAST-II [**AFII**] for systematics (Sec. 10). In the analysis, the simulated events were reweighted based on their pile-up to match the pile-up profile observed in data.

The full list of MC samples and their corresponding cross sections are given in App. **??**. The single boson and diboson cross sections are calculated to NNLO [**bosonXsec**]. The $t\bar{t}$ cross section is calculated at NNLO in QCD including resummation of NNLL soft gluon terms for a top-quark mass of 172.5 GeV [**ttXsec**]. The $t\bar{t}H$ and $t\bar{t}V$ are normalized to NLO cross sections according to [**HiggsBR**] and [**ttVXsec**]. The $t$-channel and $s$-channel single top cross sections are calculated at NLO with Hathor v2.1 [**Hather1**, **Hather2**], while the $Wt$ channel is calculated at NLO+NNLL [**WtXsec**].

# 4 Object reconstruction

In this section, various objects used in this analysis are defined, namely jets, electrons, muons, hadronically decaying taus and missing transverse energy.

## 4.1 Jets

Jets are reconstructed using the anti-$k_t$ algorithm [**antikt**] with a distance parameter $R = 0.4$ applied to the particle flow candidates. Only jets with $p_T > 25$ GeV and $|\eta| < 4.5$ are considered by the analysis. To suppress jets produced in additional pile-up interactions, jets with $p_T < 60$ GeV and $|\eta| < 2.4$ are required to have a Jet Vertex Tagger (JVT [**JVT**]) parameter larger than 0.2 (Medium working point). The JVT is the output of the jet vertex tagger algorithm used to identify and select jets originating from the hard-scatter interaction through the use of tracking and vertexing information. About 10% of selected jets in the signal are in the forward detector region. Figure **??** shows the $\eta$ of the 4th leading jet in the analysis. After the above selection and overlap removal, a "jet cleaning" cut is applied on all the jets, and the events with jets not passing this cut are discarded.

## 4.2 b-tagging

The DL1r [**btag1**] algorithm is used to identify the jets initiated by $b$-quarks. A working point corresponding to an average efficiency of 70% for jets containing $b$-quarks is chosen.

## 4.3 Electrons

Electron candidates are identified by tracks reconstructed in the inner detector and the matched cluster of energy deposited in the electromagnetic calorimeter. Electrons candidates are required to have $E_T > 15$ GeV and $|\eta| < 2.47$. The transition region, $1.37 < |\eta| < 1.52$, between the barrel and end-cap calorimeters is excluded. They are further required to pass a `loose + b-layer` likelihood-based identification point [**ElectronID**] and a `FCLoose` isolation working point [**IsolationWP**]. The electrons are further removed if its cluster is affected by the presence of a dead frontend board in the first or second sampling or by the presence of a dead high voltage region affecting the three samplings or by the presence of a masked cell in the core.

## 4.4 Muons

Muon reconstruction begins with tracks reconstructed in the MS and is matched to tracks reconstructed in the inner detector. Muon candidates are required to have $p_T > 10$ GeV and $|\eta| < 2.5$. A `Loose` identification selection [**MuonSelectionTool**] based on the requirements on the number of hits in the ID and the MS is satisfied. A `Gradient` isolation [**IsolationWP**] criterion is also required.

## 4.5 Hadronic tau decays

The hadronic tau candidates [**tau_sys1**] are seeded by jets reconstructed by the anti-$k_t$ algorithm [**antikt**], which is applied on calibrated topo clusters [**topocluster**] with a distance parameter of R=0.4. They are required to have $p_T > 20$ GeV and $|\eta| < 2.5$. The transition region between the barrel and end-cap calorimeters ($1.37 < |\eta| < 1.52$) is excluded. An identification algorithm based on Recursive Neural Network [**tau_sys2**] is applied to discriminate the visible decay products of hadronically decaying tau lepton $\tau_{\text{had}}$ from jets initiated by quarks or gluons. Different RNN working points are provided and required at different levels depending on the analysis channel. The `Loose` ID taus are used for the overlap removal and missing transverse energy calculation. In the analysis event selection, the hadronic tau candidates are required to have one or three charged tracks and an absolute charge of one, and pass the `Medium` tau ID to reject the jets. For the `Medium` ID, the tau efficiency is about 75% (60%) for 1-prong (3-prong) candidates. The ID efficiencies are optimized to be flat versus the tau $p_T$ and pileup. The tau candidates are required to not overlap with a very loose electron candidate, and a dedicated BDT variable is also used to veto the taus which are actually electrons. If the $\tau_{\text{had}}$ candidate is also tagged as a $b$-jet, then this tau object is also not used. Efficiency scale factors for tau reconstruction, ID and electron BDT rejection [**TauCP**] are applied on tau candidates in MC.

## 4.6 Missing transverse energy

The missing transverse energy $E_T^{\text{miss}}$ is computed using the fully calibrated and reconstructed physics objects as described above. The TrackSoftTerm (TST) algorithm is used to compute the SoftTerm of the $E_T^{\text{miss}}$ [**MET**].

## 4.7 Overlap removal

For the objects passing the selection above, a geometric overlap removal is applied to eliminate the ambiguity in the object identification. When two objects are close geometrically with $\Delta R$ less than a

certain threshold, or satisfy some certain requirements, one of them will be removed. The overlap removal is done by the official overlap removal tool provided by ASG group. The "Standard" working point is used. The rules are discribed as follows in sequence:

- If two electrons have overlapped second-layer cluser, or shared tracks, the electron with lower $p_T$ is removed.

- $\tau_{had}$ within a $\Delta R = 0.2$ cone of an electron or muon are removed.

- If a muon sharing an ID track with an electron and the muon is calo-tagged, the muon is removed. Otherwise the electron is removed.

- Jets within a $\Delta R = 0.2$ cone of an electron are removed.

- Electrons within a $\Delta R = 0.4$ cone of a jet are removed.

- When a muon ID track is ghost associated to a jet or within a $\Delta R = 0.2$ cone of a jet, the jet is removed if it has less than 3 tracks with $p_T > 500$ MeV or has a relative small $p_T$ ($p_T^{\mu} > 0.5 p_T^{jet}$ and $p_T^{\mu} > 0.7$[the scalar sum of the $p_T$'s of the jet tracks with $p_T > 500$ MeV]).

- Muons within a $\Delta R = 0.4$ cone of a jet are removed.

- Jets within a $\Delta R = 0.2$ cone of the leading $\tau_{had}$ ($\tau_{lep}\tau_{had}$), or with the two leading $\tau_{had}$'s ($\tau_{had}\tau_{had}$), are excluded. The overlap also works for the reverted tau ID regions used in the analysis, since the tau ID information is not used.

- If a tau object is also tagged as a $b$-jet, then this tau object is removed.

Note that the $E_T^{miss}$ calculation package has its own overlap removal procedure. Taus that fail `Loose` ID are also passed to the package. Only two leading taus are considered in the calculation.

Table 2: Overview of the final states of signal events

| # of particles | | alias | b-jet | jets | lepton | taus |
|---|---|---|---|---|---|---|
| ST | $W \to l\nu$ | STL | 1 | 1 | 1 | 2 |
| | $W \to q\bar{q}$ | STH | 1 | 3 | 0 | 2 |
| TT | $W \to l\nu$ | TTL | 1 | 2 | 1 | 2 |
| | $W \to q\bar{q}$ | TTH | 1 | 4 | 0 | 2 |

Table 3: Overview of the signal regions

| # of particles | b-jet | jets | lepton | hadronic taus |
|---|---|---|---|---|
| $2lSS\tau_{\text{had}}$ | 1 | $\geq 1$ | 2 | 1 |
| $l\tau_{\text{had}}\tau_{\text{had}}$ | 1 | $\geq 1$ | 1 | 2 |
| STH $\tau_{\text{had}}\tau_{\text{had}}$ | 1 | 3 | 0 | 2 |
| TTH $\tau_{\text{had}}\tau_{\text{had}}$ | 1 | $\geq 4$ | 0 | 2 |
| STH $\tau_{\text{lep}}\tau_{\text{had}}$ | 1 | 3 | 1 | 1 |
| TTH $\tau_{\text{lep}}\tau_{\text{had}}$ | 1 | $\geq 4$ | 1 | 1 |

# 5 Reconstruction of event topology

Depending on the production modes and the decay of the $W$ boson from top quark, the analysis is split into 4 categories as shown in table 3. All of the 8 decay modes are considered in the analyses. The selection requirement dedicated for each decay mode is also listed in talbe 3. Due to the low statistics when STL cuts are applied, the ST and TTL are included in a single region ($l\tau_{\text{had}}$ for $H \to \tau_{\text{had}}\tau_{\text{had}}$ and $2lSS\tau_{\text{had}}$ for $H \to \tau_{\text{lep}}\tau_{\text{had}}$) where there is no light jet multiplicity requirement. In order to reduce the background, the $2lSS\tau_{\text{had}}$ region requires the the leptonic tau and the lepton from W decay to be of the same charge, where the "2lSS" comes from.

For the future convenience, STH $\tau_{\text{lep}}\tau_{\text{had}}$ and TTH $\tau_{\text{lep}}\tau_{\text{had}}$ are indicated by $\tau_{\text{lep}}\tau_{\text{had}}$; STH $\tau_{\text{had}}\tau_{\text{had}}$ and TTH $\tau_{\text{had}}\tau_{\text{had}}$ are indicated by $\tau_{\text{had}}\tau_{\text{had}}$; All the channels involving leptons (including $\tau_{\text{lep}}$) are indicated by leptonic channels.

To comply with the signal topology, in each channel, exactly one jet should be tagged as a $b$-jet.

In TTH channel, all jets from the top hadronic decay and the jet from $t \to Hq$, denoted as the FCNC jet, pass the jet selection, there should be at least four jets among which the one with smallest $\Delta R(p_{\text{jet}}^{\mu}, p_{\tau 1}^{\mu} + p_{\tau 2}^{\mu})$ is considered as FCNC jet. If there are more than 2 jets beside FCNC jet and $b$-jet, the jets from $W$ boson decay are chosen based on $W$ boson resonance. There is the chance that one of the jets fails the $p_{\text{T}}$ requirement and not reconstructed. This kind of events will fall into STH channel. The FCNC top resonance is still reconstructed given the big chance that the jet which is missing is from $W$ decay.

In STH events, there are 3 jets coming from top decay including the b-jet. So a Higgs resonance formed by the taus and a top resonance formed by the jets are expected.

²⁸² In STH and TTH channels , the method introduced in [**fcnc_PRD**] is used to recontruct the ditau mass and
²⁸³ momentum by taking the $\tau$ decay kinematics into account. To determine the 4-momenta of the invisible
²⁸⁴ decay products of the tau decays, the following $\chi^2$ in Eq. 3, based on the probability functions above and
²⁸⁵ the constraints from the tau mass, the Higgs mass and the measured $E_\mathrm{T}^\mathrm{miss}$, is defined,

$$
\chi^2 = \quad -2\ln\mathcal{P}_1 - 2\ln\mathcal{P}_2 + \left(\frac{m_{\tau_1}^\mathrm{fit}-1.78}{\sigma_\tau}\right)^2 + \left(\frac{m_{\tau_2}^\mathrm{fit}-1.78}{\sigma_\tau}\right)^2 + \left(\frac{m_H^\mathrm{fit}-125}{\sigma_\mathrm{Higgs}}\right)^2 +
$$
$$
\left(\frac{E_{x,\mathrm{miss}}^\mathrm{fit}-E_{x,\mathrm{miss}}}{\sigma_\mathrm{miss}}\right)^2 + \left(\frac{E_{y,\mathrm{miss}}^\mathrm{fit}-E_{y,\mathrm{miss}}}{\sigma_\mathrm{miss}}\right)^2 ,
\tag{3}
$$

²⁸⁶ where $\mathcal{P}_i(\Delta R)$ are the probability distributions of the angular distance of the visible and invisible decay
²⁸⁷ products in the tau decay, parametrized as a function of the momentum of the tau lepton. In the $\tau_\mathrm{lep}$ mode
²⁸⁸ where two neutrinos are present, it is extended to be the joint probability distribution of $\Delta R$ and $m_\mathrm{mis}$
²⁸⁹ with $m_\mathrm{mis}$ being the invariant mass of the neutrinos, denoted by $\mathcal{P}(\Delta R, m_\mathrm{mis})$. These probability density
²⁹⁰ functions are obtained from the MC simulation. Figure 2 illustrates the distributions of $\mathcal{P}(\Delta R, m_\mathrm{mis})$ for
²⁹¹ $\tau_\mathrm{lep}$, and $\mathcal{P}(\Delta R)$ for $\tau_\mathrm{had}$, with the original tau's momentum in the range 60 GeV$< p <$ 80 GeV. Figures
²⁹² **??-??** in App. **??** show the distributions for each term in Eq. 3.
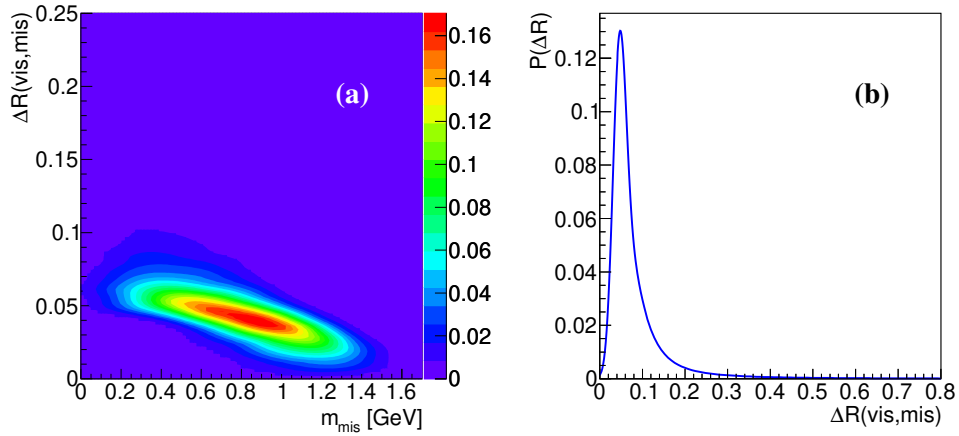


Figure 2: The distributions of (a) $\mathcal{P}(\Delta R, m_\mathrm{mis})$ for $\tau_\mathrm{lep}$, and (b) $\mathcal{P}(\Delta R)$ for $\tau_\mathrm{had}$, with the original tau's momentum in the range 60 GeV$< p <$ 80 GeV.

²⁹³ In Eq. 3, the free parameters scanned are the 4-momentum components of the invisible decay products for
²⁹⁴ each tau decay. In the $\tau_\mathrm{had}$ mode, only three momentum components are scanned since a single neutrino is
²⁹⁵ massless. $m_{\tau_{1,2}}^\mathrm{fit}$, $m_H^\mathrm{fit}$ and $E_{xy,\mathrm{miss}}^\mathrm{fit}$ are the calculated tau mass, Higgs mass, and missing transverse energy
²⁹⁶ with the scanned parameters. The corresponding mass resolutions, $\sigma_\tau$ and $\sigma_\mathrm{Higgs}$, are set to 1.8 GeV and
²⁹⁷ 20 GeV respectively. The $E_\mathrm{T}^\mathrm{miss}$ resolution is parametrized as

$$
\sigma_\mathrm{miss} = 13.1 + 0.50\sqrt{\Sigma E_\mathrm{T}},
\tag{4}
$$

²⁹⁸ where $\Sigma E_\mathrm{T}$ (in GeV) is the scalar sum of transverse energy depositions of all objects and clusters. The

299 invisible 4-momenta are obtained by minimizing the combined $\chi^2$ for each event[1]. By adding the Higgs

300 mass constraint term in the kinematic fit, not only is the Higgs mass resolution improved, but also the

301 resolutions of the Higgs boson's four-momentum, and the mass of the top from which the Higgs comes.

302 Figure 3 shows the distributions of $\chi^2$ in different regions. Good agreement between data and background

303 predictions are achieved.

/home/boyang/work/FCNCProject/FCNCAnalysis/work/StatModel/FCNCFigures/g... $lh$ 3-jet
**(a)**

$lh$ 4-jet
**(b)**

/home/boyang/work/FCNCProject/FCNCAnalysis/work/StatModel/FCNCFigures/... $hh$ 3-jet
**(c)**

$hh$ 4-jet
**(d)**
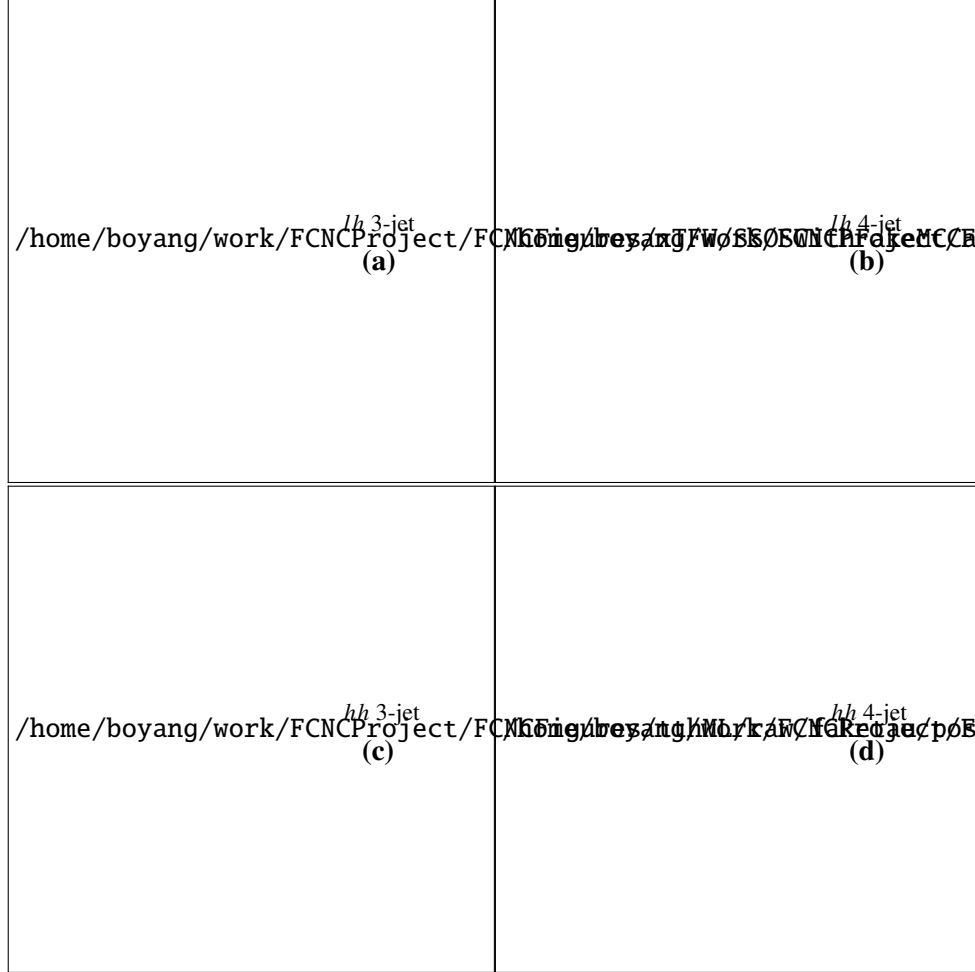
Figure 3: The distributions of $\chi^2$ in Eq. 3 in the hadronic channels.

304 In $l\tau_{\mathrm{had}}\tau_{\mathrm{had}}$ channels, a Higgs resonance formed by the taus is expected. Additionally for TTL $\tau_{\mathrm{had}}\tau_{\mathrm{had}}$

305 events, a top resonance formed by the c/u jet and Higgs is expected. Thus the invariant mass of the

306 hadronic tau candidates and the FCNC-jet is required to be less than 125GeV. Due to the large amount of

307 neutrinos produced in leptonic channels with a huge degree of freedom. The kinematic fit to reconstruct

308 the neutrinos is given up in $l\tau_{\mathrm{had}}\tau_{\mathrm{had}}$ channels. The kinematics calculated directly from visible particles

309 and $E_{\mathrm{T}}^{\mathrm{miss}}$ are used as BDT input.

---

[1] The coarse global minimum of the $\chi^2$ in Eq. 3 is first obtained by scanning the $(\eta, \phi)$ of the netrino(s) from one tau, and repeating for the other tau. Then a final minimum is obtained around it with the MINUIT packge [**MINUIT**].

With the event topology reconstructed, a number of variables are defined for signal and background separation. Their distributions can be found in Sec. 8, and some of their explanations are as follows. In the following explanations, tau candidates or di-tau point to the visible decay product of both $\tau_{\text{had}}$ and $\tau_{\text{lep}}$.

1. $E^T_{miss}$ is the missing transverse momentum.

2. $p_{T,\tau}$ is the transverse momentum of the leading tau candidate.

3. $p_{T,sub-\tau}$ is the transverse momentum of the sub-leading tau candidate.

4. $p_{T,l}$ is the transverse momentum of the leading lepton.

5. $p_{T,sub-l}$ is the transverse momentum of the sub-leading lepton.

6. $\chi^2$ is derived from kinematic fitting for the neutrinos.

7. $m_{t,SM}$ is the invariant mass of the $b$-jet and the two jets from the $W$ decay, and reflects the top mass in the decay $t \rightarrow Wb \rightarrow j_1 j_2 b$. This variable is only defined for the 4-jet STH and TTH events.

8. $m^T_W$ is the transverse mass calculated from the lepton and $E^{\text{miss}}_{\text{T}}$ in the leptonic channels, defined as

$$m^T_W = \sqrt{2p_{\text{T,lep}}E^{\text{miss}}_{\text{T}}\left(1 - \cos\Delta\phi_{\text{lep,miss}}\right)}. \tag{5}$$

9. $m_{\tau,\tau}$ is the invariant mass of the tau candidates and reconstructed neutrinos in STH and TTH channels.

10. $m_W$ is the reconstructed invariant mass of the hadronic $W$ boson from SM top quark.

11. $m_{t,FCNC}$ is the visible invariant mass of the FCNC-decaying top quark reconstructed from di-tau candidates, FCNC-jet and reconstructed neutrinos.

12. $m_{\tau\tau,vis}$ is the visible invariant mass of the two tau candidates

13. $p_{T,\tau\tau,vis}$ is the $p_{\text{T}}$ of the di-tau candidates.

14. $m_{t,FCNC,vis}$ is the reconstructed invariant mass of the FCNC-decaying top quark.

15. $m_{t,SM,vis}$ is the invariant mass of the lepton (the lepton far-away from tau candidate in the 2lSS channel) and the b-jet, which reflects the visible SM top mass.

16. $M(\tau\tau light-jet, min)$ is the invariant mass of the two tau candidates (include leptonic tau) and the light-flavor jet, minimized by choosing different jet.

17. $M(light-jet, light-jet, min)$ is the invariant mass of two light-flavor jet, minimized by choosing different jets.

18. $E_{miss}^T$ centrality is a measure of how central the $E_T^{\text{miss}}$ lies between the two tau candidates in the transverse plane, and is defined as

$$E_T^{\text{miss}} \text{ centrality} = (x + y)/\sqrt{x^2 + y^2},$$
$$\text{with } x = \frac{\sin(\phi_{\text{miss}} - \phi_{\tau_1})}{\sin(\phi_{\tau_2} - \phi_{\tau_1})}, y = \frac{\sin(\phi_{\tau_2} - \phi_{\text{miss}})}{\sin(\phi_{\tau_2} - \phi_{\tau_1})}, \tag{6}$$

19. $E_{v,i}/E_{\tau,i}, i = 1, 2$ is the momentum fraction carried by the visible decay products from the tau mother. It is based on the best-fit 4-momentum of the neutrino(s) according to the event reconstruction algorithm in this section. For the $\tau_{\text{had}}$ decay mode, the visible decay products carry most of the tau energy since there is only a single neutrino in the final state, which is evident in the excess around 1 in Fig. 4.

20. $\Delta R(l + b - jet, \tau + \tau)$ is the angular distance between the lepton+b-jet and di-tau candidates.

21. $\Delta R(l, b - jet)$ is the angular distance between the lepton and b-jet.

22. $\Delta R(\tau, b - jet)$ is the angular distance between the tau and b-jet.

23. $\eta_{\tau,max}$ is the larger polar angle among the tau candidates.

24. $\Delta R(l, \tau)$ is the angular distance between the lepton and the closest tau candidate in the leptonic channels.

25. $\Delta R(\tau, fcnc - j)$ is the angular distance between the tau and the reconstructed fcnc jet.

26. $\Delta R(\tau, \tau)$ is the angular distance between two tau candidates.

27. $\Delta R(\tau, light - jet, min)$ is the angular distance between the closest tau candidate and light-flavor jet.

28. $\Delta\phi(\tau\tau, P_{miss}^T)$ is the azimuthal angle between the $E_T^{\text{miss}}$ and di-tau $p_T$.

# 6 Selection of events

In the leptonic channels, exactly one lepton with $p_T > 10$ GeV passing `Tight` ID as defined in Sec. 4 is required. Further more, the $p_T$ of the lepton is required to be 1 GeV above the trigger threshold. After the objetct reconstruction and overlap removal. The events are categorized according to tab. **??**.

In the $\tau_{had}\tau_{had}$ channel, no leptons (as defined in Sec. 4) should be present in the event, and the two tau candidates with the highest $p_T$ are chosen. They should also pass the `Medium` tau ID and overlap removal. To account for the trigger thresholds, the two hadronic taus in $\tau_{had}\tau_{had}$ are requried to pass the $p_T > 40$ GeV and $p_T > 30$ GeV cuts.

## 6.1 Trigger

In the leptonic channels, the single-lepton triggers are required to select the candidate events. In general, the lowest unprescaled triggers are used in both data-taking periods:

Single-lepton triggers in 2015:

- `HLT_e24_lhmedium_L1EM20VH`, or `HLT_e60_lhmedium`, or `HLT_e120_lhloose`

- `HLT_mu20_iloose_L1MU15`, or `HLT_mu50`

Single-lepton triggers in 2016:

- `HLT_e26_lhtight_nod0_ivarloose`, or `HLT_e60_lhmedium_nod0`, or `HLT_e140_lhloose_nod0`

- `HLT_mu26_ivarmedium`, or `HLT_mu50`

The trigger matching between the offline and trigger level lepton objects is also required for the corresponding leptons selected for the analysis. The minimum offline lepton $p_T$ should be 1 GeV above the trigger threshold. For the $\tau_\mu\tau_{had}$ channel in 2016, the offline muon $p_T$ is 2 GeV above the trigger threshold due to the trigger scale factors' binning[2].

In the $\tau_{had}\tau_{had}$ channel, for the 2015 data-taking period, events are required to pass the triggers:

- `HLT_tau35_medium1_tracktwo_tau25_medium1_tracktwo_L1TAU20IM_2TAU12IM`

- `HLT_tau35_loose1_tracktwo_tau25_loose1_tracktwo`

---

[2] The trigger $p_T$ cuts on the leptons are independent of and additional to the other $p_T$ cuts introduced previously. For example, the $p_T$ cuts used in the overlap removal are still as those in Sec. 4. It is also the case for the cuts introduced in the AOD derivations (Sec. 6.2).

For the 2016 data-taking, events are required to pass the triggers:

- `HLT_tau35_loose1_tracktwo_tau25_loose1_tracktwo`

- `HLT_tau35_medium1_tracktwo_tau25_medium1_tracktwo`

- `HLT_tau80_medium1_TAU60_tau50_medium1_L1TAU12`

- `HLT_tau35_medium1_tracktwo_tau25_medium1_tracktwo`

For the 2017 data-taking, events are required to pass the triggers:

- `HLT_tau35_medium1_tracktwo_tau25_medium1_tracktwo`

- `HLT_tau35_medium1_tracktwo_tau25_medium1_tracktwo_03dR30_L1DR_TAU20ITAU12I_J25`

- `HLT_tau35_medium1_tracktwo_tau25_medium1_tracktwo_L1DR_TAU20ITAU12I_J25`

- `HLT_tau40_medium1_tracktwo_tau35_medium1_tracktwo`

- `HLT_tau80_medium1_tracktwo_L1TAU60_tau50_medium1_tracktwo_L1TAU12`

- `HLT_tau80_medium1_tracktwo_L1TAU60_tau35_medium1_tracktwo`
  `_L1TAU12IM_L1TAU60_DR_TAU20ITAU12I`

- `HLT_tau80_medium1_tracktwo_L1TAU60_tau50_medium1_tracktwo_L1TAU12`

- `HLT_tau80_medium1_tracktwo_L1TAU60_tau35_medium1_tracktwo`
  `_L1TAU12IM_L1TAU60_DR_TAU20ITAU12I`

- `HLT_tau80_medium1_tracktwo_L1TAU60_tau60_medium1_tracktwo_L1TAU40`

For the 2018 data-taking, events are required to pass the triggers:

- `HLT_tau80_medium1_tracktwoEF_L1TAU60_tau60_medium1_tracktwoEF_L1TAU40`

- `HLT_tau80_medium1_tracktwoEF_L1TAU60_tau35_medium1_tracktwoEF`
  `_L1TAU12IM_L1TAU60_DR_TAU20ITAU12I`

- `HLT_tau80_mediumRNN_tracktwoMVA_L1TAU60_tau60_mediumRNN_tracktwoMVA_L1TAU40`

- `HLT_tau80_mediumRNN_tracktwoMVA_L1TAU60_tau35_mediumRNN_tracktwoMVA`
  `_L1TAU12IM_L1TAU60_DR_TAU20ITAU12I`

- `HLT_tau40_medium1_tracktwoEF_tau35_medium1_tracktwoEF`

- `HLT_tau35_medium1_tracktwoEF_tau25_medium1_tracktwoEF`
  `_L1DR_TAU20ITAU12I_J25`

407 • `HLT_tau40_mediumRNN_tracktwoMVA_tau35_mediumRNN_tracktwoMVA`

408 • `HLT_tau35_mediumRNN_tracktwoMVA_tau25_mediumRNN_tracktwoMVA`
409 `_L1DR_TAU20ITAU12I_J25`

410 is required. The two $\tau_{\text{had}}$ candidates are matched to the respective legs of the di-tau trigger using the
411 individual single tau trigger objects. The $p_T$ thresholds are chosen such that the selected $\tau_{\text{had}}$ candidate
412 $p_T$ already lies in the plateau of the respective trigger efficiency curve. Due to the rising instantaneous
413 luminosity, the trigger used in the 2016 data taking includes a requirement for an additional level-1
414 calorimeter trigger jet with $p_T > 25\,\text{GeV}$ and $|\eta| < 3.2$. The leading jet in the 2016 events is required to
415 be matched within $\Delta R < 0.4$ with the jet ROI that fulfilled the jet part of the trigger criteria (trigger jet).
416 Figure **??** shows the turn-on curves of the additional jet as in [**Htautau**], and the leading jet $p_T$ in the
417 $\tau_{\text{had}}\tau_{\text{had}}$ channel. A cut of $p_T^{\text{L1jet}} > 50\,\text{GeV}$ is required on the trigger jet, and a leading-jet $p_T > 60\,\text{GeV}$
418 cut is applied to remove the effect of turn on curve.

## 6.2 Event cuts and regions

420 A number of event cuts are applied before getting to the signal enhanced regions with the back-
421 ground suppressed. Then the DAOD_HIGG8D1 (DAOD_HIGG4D3) derivation is feed to `ttHMultiAna`
422 (`xTauFramework`) to produce n-tuples for analysis. The list of event-level selection criteria is as follows:

423 1. DAOD_HIGG8D1 (leptonic channels) and DAOD_HIGG4D3 ($\tau_{\text{had}}\tau_{\text{had}}$) derivations are used for
424 this analysis. At the derivation level, the following cuts are applied:

425 • In DAOD_HIGG8D1, trigger skimming: all election, muon, tau triggers; Offline skimming:
426 at least 2 light leptons or at least 1 lepton plus 1 tau.

427 • In DAOD_HIGG4D3, no trigger skimming. Offline skimming: 2taus

428 2. At the `xTauFramework` level, skim cuts are applied to reduce the ntuple size:

429 • No leptons, at least 1 medium tau and 1 loose tau, at least 3 jets with $p_T > 30$ GeV, $|\eta| < 4.5$
430 and passing either central or forward JVT cuts and with at least 1 b-tagged, pass di-tau trigger,
431 LooseBad Event Cleaning, leading tau $p_T > 40$ GeV, sub-leading tau $p_T > 30$ GeV, two taus
432 comes from a single vertex, leading jet $p_T > 60$ GeV, leading jet $|\eta| < 3.2$, $E_T^{\text{miss}} > 15$ GeV.
433 In the case of data, GRL cut as defined in Sec. 3.2 is also applied.

434 3. At the `ttHMultiAna` level, skim cuts [**ATL-COM-PHYS-2018-410**] are applied to reduce the ntuple
435 size.

436 4. A least one primary vertex exists in the event. The primary vertex is defined as the vertex that has
437 the largest sum of track $p_T^2$ associated to it, and has at least 4 tracks with $|z_0| < 100$ mm.

5. The tau candidtes expected from Higgs decay should pass the `Medium` ID and the other quality cuts in Sec. 4.

6. It is required that the tau objects are not *b*-tagged, otherwise the event is rejected.

7. Exactly one *b*-tagged jets with $p_T > 30$ GeV and $|\eta| < 2.5$.

8. Considering the di-tau are from the Higgs decay, their invariant mass should satisfy 50 GeV < $m_{\tau\tau,\text{vis}} < 130$ GeV and $\Delta R(\tau, \tau) < 3.4$ in the $\tau_{\text{had}}\tau_{\text{had}}$ channel and 25 GeV < $m_{\tau\tau,\text{vis}} < 125$ GeV in leptonic channels.

9. In $l\tau_{\text{had}}\tau_{\text{had}}$ channels, the lepton and b-jet are from SM top decay, so their invarian mass is expected to be smaller or around top mass: $m_{t,\text{SM,vis}} < 190$ GeV.



/home/boyang/work/FCNCProject/FCNC... /home/boyang/work/FCNC...
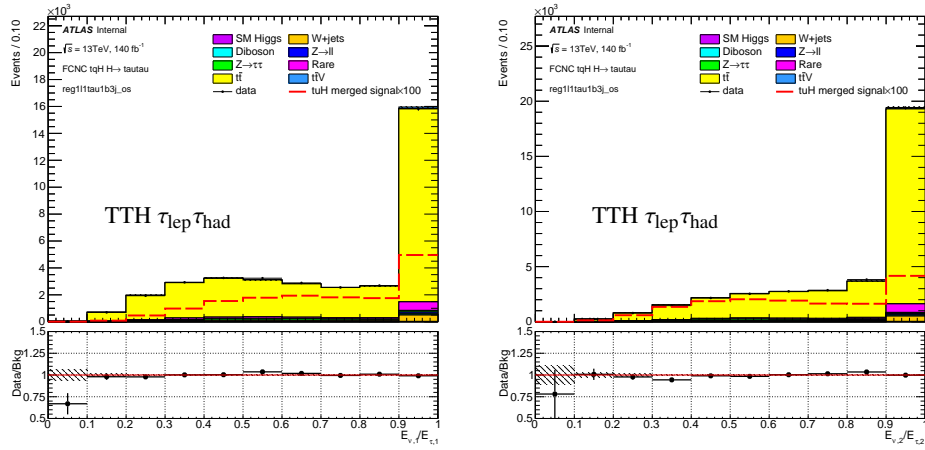
Figure 4: The distributions of $x^{\text{fit}}_{1,2}$ in the TTH $\tau_{\text{lep}}\tau_{\text{had}}$ (top) and $\tau_{\text{had}}\tau_{\text{had}}$ (bottom) channels.

The expected event yields for the backgrounds, signal and data after the above cuts are given in Tab. 4-14, with the exception for the fake background, which is estimated at a later cut stage as detailed in Sec. 8.

Table 4: The expected event yields (corresponds to 36.1 fb$^{-1}$) for different MC processes and data after each cut in the $\tau_{\text{lep}}\tau_{\text{had}}$ channel. The signal yields are obtained by assuming BR($t \to Hq$)=1%, and BR($t \to Hc$)=BR($t \to Hu$)=0.5%. The uncertainties are statistical only.

| | Top | | diboson | $Z \to \ell\ell$ |
|---|---|---|---|---|
| | real $\tau_{\text{had}}$ | fake $\tau_{\text{had}}$ | | |
| AOD | $(3.1881 \pm 0.0004) \times 10^7$ | | $(2.801 \pm 0.001) \times 10^6$ | $(1.5049 \pm 0.0005) \times 10^8$ |
| DAOD | $(1.1555 \pm 0.0002) \times 10^7$ | | $(7.186 \pm 0.004) \times 10^5$ | $(5.723 \pm 0.003) \times 10^7$ |
| skim | 76041.7 ± 145.9 | 1380820.6 ± 625.1 | 3735.5 ± 25.0 | 26761.2 ± 144.6 |
| vertex | 71579.4 ± 141.6 | 1299919.6 ± 606.6 | 3515.5 ± 24.2 | 25208.0 ± 140.3 |
| trigger | 58457.1 ± 127.9 | 1116757.0 ± 561.3 | 3094.6 ± 22.8 | 21913.8 ± 118.7 |
| tau sel. | 26798.8 ± 99.8 | 23601.1 ± 97.7 | 119.0 ± 6.5 | 579.2 ± 24.8 |
| 3jet veto | 24427.2 ± 95.5 | 20198.7 ± 90.4 | 106.7 ± 6.2 | 518.4 ± 23.5 |
| tau not $b$-tagged | 23818.9 ± 94.3 | 17991.9 ± 84.5 | 103.3 ± 6.2 | 493.3 ± 23.2 |
| $x_{1,2}^{\text{fit}}$ | 12833.8 ± 69.0 | 11784.7 ± 68.4 | 62.9 ± 3.9 | 357.0 ± 22.3 |
| $N_{\text{bjet}}$=1 | 7094.9 ± 50.7 | 7027.7 ± 52.3 | 53.7 ± 3.6 | 316.3 ± 22.0 |

| | $Z \to \tau\tau$ | $W \to l\nu$ | $t \to qH$ | data |
|---|---|---|---|---|
| AOD | $(4.491 \pm 0.006) \times 10^6$ | $(2.152 \pm 0.001) \times 10^9$ | 12126.9 ± 19.6 | $(6.32610 \pm 0.00008) \times 10^9$ |
| DAOD | $(2.951 \pm 0.005) \times 10^6$ | $(3.945 \pm 0.009) \times 10^8$ | 5691.6 ± 13.5 | $(8.0089 \pm 0.0003) \times 10^8$ |
| skim | 4251.9 ± 38.3 | 94984.2 ± 628.6 | 984.8 ± 5.7 | 1427385.0 ± 1194.7 |
| vertex | 3997.5 ± 36.8 | 89554.7 ± 615.6 | 926.0 ± 5.5 | 1419052.0 ± 1191.2 |
| trigger | 2471.5 ± 26.4 | 77051.1 ± 535.5 | 610.4 ± 4.5 | 1272074.0 ± 1127.9 |
| tau sel. | 998.5 ± 25.6 | 1851.4 ± 146.2 | 197.0 ± 2.9 | 55068.0 ± 234.7 |
| 3jet veto | 910.9 ± 23.4 | 1672.9 ± 143.3 | 169.8 ± 2.8 | 48681.0 ± 220.6 |
| tau not $b$-tagged | 901.1 ± 23.0 | 1597.1 ± 142.7 | 166.8 ± 2.7 | 45319.0 ± 212.9 |
| $x_{1,2}^{\text{fit}}$ | 875.4 ± 22.8 | 1073.8 ± 137.0 | 163.8 ± 2.7 | 27633.0 ± 166.2 |
| $N_{\text{bjet}}$=1 | 757.3 ± 20.8 | 1019.7 ± 136.8 | 147.9 ± 2.5 | 16882.0 ± 129.9 |

449 The summery of the yields and signal significance in leptonic channels are shown in table **??** and **??**.

Table 5: The expected event yields (corresponds to 140 fb$^{-1}$) for different MC processes and data after the cuts applied before the n-tuples produced by the **xTauFramework**. The signal yields are obtained by assuming BR($t \rightarrow Hq$)=1%. The uncertainties are statistical only.

| cut | diboson | fcnc prod ch | fcnc uh qq | wjet | data |
|---|---|---|---|---|---|
| Total Events | $(2.45 \pm 0.00) \times 10^7$ | $1060.00 \pm 0.00$ | $25588.00 \pm 0.00$ | $(1.24 \pm 0.00) \times 10^{11}$ | $(6.35 \pm 0.00) \times 10^9$ |
| DAOD | $(3.46 \pm 0.00) \times 10^6$ | $668.25 \pm 0.00$ | $14215.19 \pm 0.00$ | $(3.46 \pm 0.00) \times 10^9$ | $(5.29 \pm 0.00) \times 10^8$ |
| skim | $69.04 \pm 1.68$ | $39.23 \pm 0.35$ | $611.11 \pm 5.42$ | $451.31 \pm 14.31$ | $(1.32 \pm 0.00) \times 10^5$ |
| LooseBad Event Cleaning | $68.60 \pm 1.67$ | $39.05 \pm 0.35$ | $608.35 \pm 5.40$ | $448.09 \pm 14.28$ | $(1.30 \pm 0.00) \times 10^5$ |
| Tau pT cut | $48.63 \pm 1.34$ | $30.88 \pm 0.31$ | $455.46 \pm 4.68$ | $284.66 \pm 12.34$ | $65257.00 \pm 255.45$ |
| Di-tau common Vx cut | $48.19 \pm 1.33$ | $30.81 \pm 0.31$ | $454.06 \pm 4.67$ | $276.79 \pm 12.20$ | $60090.00 \pm 245.13$ |
| Leading jet cut | $46.22 \pm 1.29$ | $30.27 \pm 0.31$ | $446.86 \pm 4.63$ | $261.00 \pm 11.85$ | $55873.00 \pm 236.37$ |
| MET cut | $43.76 \pm 1.25$ | $27.92 \pm 0.30$ | $399.92 \pm 4.38$ | $238.83 \pm 7.65$ | $46107.00 \pm 214.73$ |
| trigger matching | $39.19 \pm 2.04$ | $25.24 \pm 0.43$ | $368.62 \pm 4.27$ | $201.55 \pm 20.53$ | $46107.00 \pm 214.73$ |
| n tracks = 1,3 | $30.98 \pm 1.73$ | $22.38 \pm 0.41$ | $319.22 \pm 3.97$ | $144.95 \pm 18.69$ | $26148.00 \pm 161.70$ |

| cut | fcnc ch lv | fcnc prod uh | smhiggs | zll |
|---|---|---|---|---|
| Total Events | $12299.39 \pm 0.00$ | $5271.38 \pm 0.00$ | $(1.32 \pm 0.00) \times 10^6$ | $(5.56 \pm 0.00) \times 10^9$ |
| DAOD | $5590.81 \pm 0.00$ | $3291.00 \pm 0.00$ | $(4.56 \pm 0.00) \times 10^5$ | $(2.77 \pm 0.00) \times 10^8$ |
| skim | $149.90 \pm 2.15$ | $185.92 \pm 1.70$ | $110.18 \pm 1.42$ | $9.36 \pm 0.95$ |
| LooseBad Event Cleaning | $149.26 \pm 2.14$ | $183.98 \pm 1.69$ | $109.70 \pm 1.42$ | $9.36 \pm 0.95$ |
| Tau pT cut | $113.67 \pm 1.87$ | $150.17 \pm 1.52$ | $84.64 \pm 1.26$ | $7.07 \pm 0.90$ |
| Di-tau common Vx cut | $113.49 \pm 1.87$ | $149.92 \pm 1.52$ | $84.35 \pm 1.26$ | $6.73 \pm 0.88$ |
| Leading jet cut | $109.12 \pm 1.83$ | $147.59 \pm 1.51$ | $80.68 \pm 1.22$ | $5.56 \pm 0.65$ |
| MET cut | $104.39 \pm 1.79$ | $137.01 \pm 1.46$ | $75.62 \pm 1.18$ | $4.50 \pm 0.62$ |
| trigger matching | $101.25 \pm 1.80$ | $128.57 \pm 2.13$ | $72.23 \pm 1.97$ | $3.11 \pm 1.47$ |
| n tracks = 1,3 | $88.17 \pm 1.68$ | $111.65 \pm 1.98$ | $63.44 \pm 1.87$ | $1.35 \pm 0.23$ |

| cut | fcnc ch qq | fcnc uh lv | top | ztautau |
|---|---|---|---|---|
| Total Events | $25591.91 \pm 0.00$ | $12297.07 \pm 0.00$ | $(4.29 \pm 0.00) \times 10^8$ | $(1.92 \pm 0.00) \times 10^9$ |
| DAOD | $14182.99 \pm 0.00$ | $5645.15 \pm 0.00$ | $(9.61 \pm 0.00) \times 10^7$ | $(2.13 \pm 0.00) \times 10^7$ |
| skim | $623.70 \pm 6.32$ | $140.81 \pm 2.08$ | $16614.80 \pm 58.13$ | $2275.01 \pm 26.63$ |
| LooseBad Event Cleaning | $620.68 \pm 6.30$ | $139.89 \pm 2.07$ | $16533.76 \pm 57.98$ | $2261.00 \pm 26.60$ |
| Tau pT cut | $463.75 \pm 5.45$ | $105.99 \pm 1.81$ | $10632.17 \pm 45.97$ | $1439.59 \pm 12.62$ |
| Di-tau common Vx cut | $461.83 \pm 5.44$ | $105.54 \pm 1.80$ | $10447.76 \pm 45.53$ | $1431.03 \pm 12.58$ |
| Leading jet cut | $454.54 \pm 5.39$ | $101.89 \pm 1.77$ | $10200.06 \pm 45.03$ | $1339.92 \pm 10.98$ |
| MET cut | $408.09 \pm 5.11$ | $97.18 \pm 1.73$ | $9428.60 \pm 42.74$ | $1196.00 \pm 10.04$ |
| trigger matching | $382.68 \pm 5.03$ | $92.98 \pm 1.72$ | $5118.07 \pm 28.24$ | $1478.04 \pm 25.18$ |
| n tracks = 1,3 | $333.62 \pm 4.70$ | $81.22 \pm 1.60$ | $3733.69 \pm 23.89$ | $1293.72 \pm 23.13$ |

Table 6: The expected event yields (corresponds to 140 fb$^{-1}$) for different MC processes and data after each cut in the STH $\tau_{\text{had}}\tau_{\text{had}}$ channel. The signal yields are obtained by assuming BR($t \rightarrow Hq$)=1%. The uncertainties are statistical only.

| cut | diboson | fcnc prod ch | fcnc uh qq | wjet | data |
|---|---|---|---|---|---|
| 2 medium OS tau 2 light-j | 9.15 ± 1.15 | 9.38 ± 0.29 | 75.31 ± 2.21 | 26.15 ± 8.94 | 3491.00 ± 59.08 |
| true taus | 8.10 ± 1.01 | 9.33 ± 0.29 | 71.85 ± 2.17 | 0.23 ± 0.17 | 3491.00 ± 59.08 |
| jet pt cut | 8.10 ± 1.01 | 9.33 ± 0.29 | 71.85 ± 2.17 | 0.23 ± 0.17 | 3491.00 ± 59.08 |
| bjet pt eta cut | 7.95 ± 1.00 | 8.90 ± 0.28 | 69.01 ± 2.14 | 0.23 ± 0.17 | 3121.00 ± 55.87 |
| tautau vis mass > 50 | 7.26 ± 0.97 | 8.75 ± 0.28 | 68.67 ± 2.13 | 0.23 ± 0.17 | 2710.00 ± 52.06 |
| tautau vis mass < 130 | 6.64 ± 0.96 | 8.54 ± 0.28 | 68.60 ± 2.13 | 0.23 ± 0.17 | 1875.00 ± 43.30 |
| drtautau > 3.4 | 6.64 ± 0.96 | 8.54 ± 0.28 | 68.50 ± 2.13 | 0.23 ± 0.17 | 1856.00 ± 43.08 |

| cut | fcnc ch lv | fcnc prod uh | smhiggs | zll |
|---|---|---|---|---|
| 2 medium OS tau 2 light-j | 25.43 ± 1.03 | 43.13 ± 1.41 | 19.73 ± 0.97 | 0.35 ± 0.22 |
| true taus | 24.68 ± 1.01 | 42.58 ± 1.41 | 19.63 ± 0.97 | 0.23 ± 0.17 |
| jet pt cut | 24.68 ± 1.01 | 42.58 ± 1.41 | 19.63 ± 0.97 | 0.23 ± 0.17 |
| bjet pt eta cut | 23.51 ± 0.99 | 41.29 ± 1.39 | 18.20 ± 0.94 | 0.23 ± 0.17 |
| tautau vis mass > 50 | 23.11 ± 0.98 | 39.87 ± 1.37 | 17.73 ± 0.94 | 0.23 ± 0.17 |
| tautau vis mass < 130 | 20.07 ± 0.92 | 38.57 ± 1.36 | 17.61 ± 0.94 | 0.23 ± 0.17 |
| drtautau > 3.4 | 20.00 ± 0.92 | 38.56 ± 1.36 | 17.60 ± 0.94 | 0.23 ± 0.17 |

| cut | fcnc ch qq | fcnc uh lv | top | ztautau |
|---|---|---|---|---|
| 2 medium OS tau 2 light-j | 74.20 ± 2.39 | 25.65 ± 0.98 | 723.83 ± 11.95 | 579.17 ± 18.36 |
| true taus | 71.97 ± 2.36 | 25.04 ± 0.97 | 432.75 ± 9.36 | 572.12 ± 18.28 |
| jet pt cut | 71.97 ± 2.36 | 25.04 ± 0.97 | 432.75 ± 9.36 | 572.12 ± 18.28 |
| bjet pt eta cut | 69.38 ± 2.32 | 24.06 ± 0.95 | 412.98 ± 9.18 | 529.87 ± 16.43 |
| tautau vis mass > 50 | 69.01 ± 2.31 | 23.66 ± 0.94 | 390.94 ± 8.96 | 471.80 ± 15.97 |
| tautau vis mass < 130 | 68.94 ± 2.31 | 20.40 ± 0.87 | 239.37 ± 6.90 | 459.53 ± 15.77 |
| drtautau > 3.4 | 68.94 ± 2.31 | 20.33 ± 0.87 | 237.10 ± 6.87 | 459.50 ± 15.77 |

Table 7: The expected event yields (corresponds to 36.1 fb$^{-1}$) for different MC processes and data after each cut in the TTH $\tau_{had}\tau_{had}$ channel. The signal yields are obtained by assuming BR($t \rightarrow Hq$)=1%. The uncertainties are statistical only.

| cut | diboson | fcnc prod ch | fcnc uh qq | wjet | data |
|---|---|---|---|---|---|
| 2 medium OS tau 3light-j 1b-j | 14.69 ± 1.15 | 9.49 ± 0.31 | 180.65 ± 3.34 | 21.49 ± 3.76 | 2897.00 ± 53.82 |
| true taus | 12.44 ± 0.81 | 9.40 ± 0.31 | 174.68 ± 3.29 | 0.30 ± 0.18 | 2897.00 ± 53.82 |
| jet pt cut | 12.44 ± 0.81 | 9.40 ± 0.31 | 174.68 ± 3.29 | 0.30 ± 0.18 | 2897.00 ± 53.82 |
| bjet pt eta cut | 11.52 ± 0.77 | 8.85 ± 0.29 | 166.93 ± 3.23 | 0.30 ± 0.18 | 2653.00 ± 51.51 |
| tautau vis mass > 50 | 10.08 ± 0.73 | 8.61 ± 0.29 | 165.48 ± 3.21 | 0.30 ± 0.18 | 2307.00 ± 48.03 |
| tautau vis mass < 130 | 9.25 ± 0.72 | 8.44 ± 0.29 | 165.15 ± 3.21 | 0.30 ± 0.18 | 1558.00 ± 39.47 |
| drtautau > 3.4 | 9.25 ± 0.72 | 8.44 ± 0.29 | 164.89 ± 3.21 | 0.30 ± 0.18 | 1542.00 ± 39.27 |

| cut | fcnc ch lv | fcnc prod uh | smhiggs | zll |
|---|---|---|---|---|
| 2 medium OS tau 3light-j 1b-j | 28.65 ± 1.03 | 47.83 ± 1.54 | 23.97 ± 1.39 | 0.32 ± 0.13 |
| true taus | 28.19 ± 1.02 | 47.13 ± 1.53 | 22.88 ± 1.29 | 0.30 ± 0.18 |
| jet pt cut | 28.19 ± 1.02 | 47.13 ± 1.53 | 22.88 ± 1.29 | 0.30 ± 0.18 |
| bjet pt eta cut | 27.08 ± 1.00 | 45.07 ± 1.51 | 20.63 ± 1.22 | 0.30 ± 0.18 |
| tautau vis mass > 50 | 26.30 ± 0.98 | 43.52 ± 1.48 | 20.18 ± 1.22 | 0.30 ± 0.18 |
| tautau vis mass < 130 | 22.29 ± 0.90 | 42.81 ± 1.47 | 19.86 ± 1.22 | 0.30 ± 0.18 |
| drtautau > 3.4 | 22.22 ± 0.90 | 42.75 ± 1.47 | 19.85 ± 1.22 | 0.30 ± 0.18 |

| cut | fcnc ch qq | fcnc uh lv | top | ztautau |
|---|---|---|---|---|
| 2 medium OS tau 3light-j 1b-j | 181.51 ± 3.91 | 29.03 ± 1.06 | 790.24 ± 12.43 | 436.60 ± 13.11 |
| true taus | 176.21 ± 3.86 | 28.37 ± 1.05 | 414.73 ± 9.02 | 429.82 ± 13.01 |
| jet pt cut | 176.21 ± 3.86 | 28.37 ± 1.05 | 414.73 ± 9.02 | 429.82 ± 13.01 |
| bjet pt eta cut | 167.96 ± 3.72 | 26.92 ± 1.03 | 395.17 ± 8.84 | 389.90 ± 11.79 |
| tautau vis mass > 50 | 165.44 ± 3.69 | 26.14 ± 1.01 | 367.07 ± 8.38 | 336.68 ± 11.46 |
| tautau vis mass < 130 | 165.44 ± 3.69 | 22.19 ± 0.94 | 215.20 ± 6.62 | 328.07 ± 11.38 |
| drtautau > 3.4 | 165.44 ± 3.69 | 22.14 ± 0.94 | 213.75 ± 6.60 | 328.36 ± 11.38 |

Table 8: cutflow all

|  | SM Higgs | W+jets | Diboson | $Z \to ll$ |
|---|---|---|---|---|
| n-tuple | 14625.17 ± 91.16 | 1566592.64 ± 7205.54 | 213685.40 ± 271.88 | 4636927.85 ± 8294.85 |
| pass trigger | 14059.18 ± 89.56 | 1537607.58 ± 7134.23 | 204530.24 ± 270.49 | 4337263.09 ± 8032.82 |
| leadtauOLR | 13770.96 ± 88.56 | 1474191.23 ± 7053.96 | 198325.54 ± 263.74 | 4119951.21 ± 7854.76 |
| subtauOLR | 13765.38 ± 88.55 | 1473902.97 ± 7053.56 | 198238.94 ± 263.64 | 4119317.61 ± 7854.42 |
| trigger match | 10066.09 ± 78.89 | 1416071.50 ± 6889.57 | 141324.18 ± 254.07 | 1764362.61 ± 3671.23 |
| tight lepton | 9778.48 ± 77.69 | 1385510.60 ± 6832.02 | 138686.48 ± 251.46 | 1745898.27 ± 3644.13 |
| PLV for lephad | 8844.03 ± 73.28 | 1250614.63 ± 6515.61 | 131408.54 ± 241.20 | 1712357.61 ± 3577.99 |
| Medium,25GeV leadtau | 7660.49 ± 67.72 | 633723.78 ± 4498.68 | 98361.94 ± 178.46 | 1487970.81 ± 3111.24 |
| Medium,25GeV subtau | 7610.88 ± 67.53 | 630850.71 ± 4490.34 | 97817.83 ± 177.88 | 1486370.34 ± 3108.40 |
| 2lSS chargeBDT | 7166.21 ± 66.53 | 630692.53 ± 4490.24 | 87682.63 ± 176.61 | 1461585.31 ± 3096.70 |
| SR+CR | 323.56 ± 7.05 | 4764.44 ± 100.85 | 846.90 ± 18.69 | 2154.49 ± 49.74 |

|  | $Z \to \tau\tau$ | Rare | $t\bar{t}$ | $t\bar{t}V$ |
|---|---|---|---|---|
| n-tuple | 410982.57 ± 2106.28 | 255371.58 ± 177.72 | 3293743.11 ± 663.22 | 18389.75 ± 14.50 |
| pass trigger | 402257.51 ± 2088.22 | 244821.58 ± 174.20 | 3137296.70 ± 647.98 | 17492.29 ± 14.17 |
| leadtauOLR | 393589.53 ± 2067.11 | 240316.57 ± 172.64 | 3081743.40 ± 642.32 | 17256.94 ± 14.06 |
| subtauOLR | 393502.11 ± 2066.96 | 240263.37 ± 172.62 | 3080893.54 ± 642.23 | 17249.13 ± 14.06 |
| trigger match | 374969.55 ± 2034.89 | 116744.43 ± 119.18 | 1469290.95 ± 440.35 | 8874.89 ± 9.95 |
| tight lepton | 361398.61 ± 1999.80 | 114193.25 ± 117.84 | 1430989.55 ± 434.42 | 8635.12 ± 9.80 |
| PLV for lephad | 306130.84 ± 1841.35 | 109983.64 ± 115.63 | 1377988.50 ± 426.23 | 8406.58 ± 9.63 |
| Medium,25GeV leadtau | 260261.36 ± 1701.23 | 95472.31 ± 107.69 | 1209179.49 ± 399.24 | 7715.94 ± 9.09 |
| Medium,25GeV subtau | 259164.05 ± 1698.34 | 95269.59 ± 107.58 | 1206366.56 ± 398.77 | 7679.14 ± 9.07 |
| 2lSS chargeBDT | 258832.22 ± 1698.19 | 85664.27 ± 101.89 | 1038613.73 ± 369.12 | 6069.71 ± 8.10 |
| SR+CR | 3395.99 ± 41.11 | 10105.97 ± 34.95 | 233280.84 ± 174.31 | 1176.69 ± 4.04 |

|  | $\bar{t}t \to bWcH$ | $cg \to tH$ | tcH merged signal | $\bar{t}t \to bWuH$ |
|---|---|---|---|---|
| n-tuple | 2697.69 ± 4.51 | 124.01 ± 0.33 | 2821.70 ± 4.53 | 2697.40 ± 4.47 |
| pass trigger | 2591.28 ± 4.43 | 119.06 ± 0.33 | 2710.34 ± 4.44 | 2592.75 ± 4.38 |
| leadtauOLR | 2561.17 ± 4.40 | 117.83 ± 0.32 | 2678.99 ± 4.42 | 2565.50 ± 4.36 |
| subtauOLR | 2554.93 ± 4.40 | 117.50 ± 0.32 | 2672.43 ± 4.41 | 2560.52 ± 4.36 |
| trigger match | 1905.99 ± 3.84 | 87.85 ± 0.28 | 1993.85 ± 3.85 | 1911.71 ± 3.80 |
| tight lepton | 1830.03 ± 3.75 | 84.22 ± 0.28 | 1914.25 ± 3.76 | 1835.41 ± 3.71 |
| PLV for lephad | 1674.71 ± 3.56 | 77.45 ± 0.26 | 1752.16 ± 3.57 | 1677.64 ± 3.52 |
| Medium,25GeV leadtau | 1452.96 ± 3.31 | 68.38 ± 0.25 | 1521.34 ± 3.32 | 1456.47 ± 3.28 |
| Medium,25GeV subtau | 1391.67 ± 3.25 | 64.96 ± 0.24 | 1456.64 ± 3.26 | 1391.88 ± 3.21 |
| 2lSS chargeBDT | 1330.55 ± 3.19 | 62.02 ± 0.24 | 1392.57 ± 3.19 | 1336.84 ± 3.15 |
| SR+CR | 520.04 ± 2.04 | 21.52 ± 0.14 | 541.56 ± 2.04 | 496.34 ± 1.96 |

|  | $ug \to tH$ | tuH merged signal | Data |
|---|---|---|---|
| n-tuple | 631.43 ± 1.70 | 3328.82 ± 4.78 | 11704069.00 ± 3421.12 |
| pass trigger | 608.67 ± 1.67 | 3201.42 ± 4.69 | 11025193.00 ± 3320.42 |
| leadtauOLR | 601.45 ± 1.66 | 3166.96 ± 4.67 | 10611339.00 ± 3257.51 |
| subtauOLR | 599.85 ± 1.66 | 3160.37 ± 4.66 | 10609326.00 ± 3257.20 |
| trigger match | 450.14 ± 1.45 | 2361.85 ± 4.06 | 6138248.00 ± 2477.55 |
| tight lepton | 431.10 ± 1.42 | 2266.51 ± 3.97 | 5936612.00 ± 2436.52 |
| PLV for lephad | 387.95 ± 1.34 | 2065.59 ± 3.77 | 5323308.00 ± 2307.23 |
| Medium,25GeV leadtau | 341.59 ± 1.25 | 1798.06 ± 3.51 | 4198878.00 ± 2049.12 |
| Medium,25GeV subtau | 326.84 ± 1.23 | 1718.72 ± 3.44 | 4189971.00 ± 2046.94 |
| 2lSS chargeBDT | 311.27 ± 1.20 | 1648.11 ± 3.37 | 3992980.00 ± 1998.24 |
| SR+CR | 109.17 ± 0.73 | 605.51 ± 2.09 | 248440.00 ± 498.44 |

Table 9: cutflow STH $\tau_{\text{lep}}\tau_{\text{had}}$ os

|  | SM Higgs | W+jets | Diboson | $Z \to ll$ |
|---|---|---|---|---|
| this region | 42.23 ± 4.06 | 1546.04 ± 72.45 | 261.45 ± 9.62 | 683.61 ± 28.69 |
| tau b-veto | 40.66 ± 3.96 | 1500.11 ± 72.24 | 252.69 ± 9.51 | 675.63 ± 28.63 |
| $MET > 20$ | 36.14 ± 3.63 | 1324.40 ± 65.48 | 223.02 ± 8.90 | 455.90 ± 23.79 |

|  | $Z \to \tau\tau$ | Rare | $t\bar{t}$ | $t\bar{t}V$ |
|---|---|---|---|---|
| this region | 1531.36 ± 32.17 | 3390.38 ± 20.40 | 51954.64 ± 82.91 | 143.35 ± 1.33 |
| tau b-veto | 1496.12 ± 31.36 | 3266.23 ± 20.03 | 49638.21 ± 81.08 | 137.44 ± 1.30 |
| $MET > 20$ | 1260.39 ± 28.13 | 3027.77 ± 19.29 | 46213.66 ± 78.23 | 130.85 ± 1.27 |

|  | $\bar{t}t \to bWcH$ | $cg \to tH$ | tcH merged signal | $\bar{t}t \to bWuH$ |
|---|---|---|---|---|
| this region | 111.45 ± 0.99 | 6.06 ± 0.08 | 117.51 ± 0.99 | 114.44 ± 0.98 |
| tau b-veto | 108.09 ± 0.97 | 5.91 ± 0.08 | 114.01 ± 0.98 | 110.93 ± 0.96 |
| $MET > 20$ | 96.35 ± 0.91 | 5.27 ± 0.07 | 101.62 ± 0.92 | 98.84 ± 0.90 |

|  | $ug \to tH$ | tuH merged signal | Data |
|---|---|---|---|
| this region | 30.89 ± 0.41 | 145.33 ± 1.06 | 57506.00 ± 239.80 |
| tau b-veto | 29.91 ± 0.40 | 140.84 ± 1.04 | 54969.00 ± 234.45 |
| $MET > 20$ | 27.00 ± 0.38 | 125.84 ± 0.98 | 50560.00 ± 224.86 |

Table 10: cutflow STH $\tau_{\text{lep}}\tau_{\text{had}}$ ss

|  | SM Higgs | W+jets | Diboson | $Z \to ll$ |
|---|---|---|---|---|
| this region | 14.01 ± 2.12 | 908.46 ± 44.90 | 98.10 ± 8.06 | 227.84 ± 20.27 |
| tau b-veto | 13.31 ± 2.09 | 873.18 ± 44.57 | 95.87 ± 8.05 | 222.30 ± 20.23 |
| $MET > 20$ | 12.91 ± 2.09 | 739.05 ± 39.22 | 87.60 ± 7.87 | 170.82 ± 18.23 |

|  | $Z \to \tau\tau$ | Rare | $t\bar{t}$ | $t\bar{t}V$ |
|---|---|---|---|---|
| this region | 24.42 ± 3.44 | 339.72 ± 6.31 | 5144.83 ± 26.08 | 53.78 ± 0.68 |
| tau b-veto | 23.33 ± 3.41 | 303.12 ± 5.97 | 4268.68 ± 23.85 | 50.78 ± 0.66 |
| $MET > 20$ | 20.68 ± 2.56 | 274.49 ± 5.68 | 3886.87 ± 22.76 | 47.57 ± 0.64 |

|  | $\bar{t}t \to bWcH$ | $cg \to tH$ | tcH merged signal | $\bar{t}t \to bWuH$ |
|---|---|---|---|---|
| this region | 56.23 ± 0.59 | 1.44 ± 0.03 | 57.68 ± 0.59 | 58.58 ± 0.60 |
| tau b-veto | 54.46 ± 0.58 | 1.41 ± 0.03 | 55.87 ± 0.58 | 56.79 ± 0.59 |
| $MET > 20$ | 49.84 ± 0.55 | 1.31 ± 0.03 | 51.15 ± 0.55 | 52.11 ± 0.56 |

|  | $ug \to tH$ | tuH merged signal | Data |
|---|---|---|---|
| this region | 7.95 ± 0.17 | 66.53 ± 0.62 | 7105.00 ± 84.29 |
| tau b-veto | 7.74 ± 0.17 | 64.53 ± 0.61 | 6176.00 ± 78.59 |
| $MET > 20$ | 7.14 ± 0.17 | 59.25 ± 0.59 | 5434.00 ± 73.72 |

Table 11: cutflow TTH $\tau_{\text{lep}}\tau_{\text{had}}$ os

|  | SM Higgs | W+jets | Diboson | $Z \rightarrow ll$ |
|---|---|---|---|---|
| this region | 74.66 ± 3.47 | 915.11 ± 23.28 | 249.68 ± 10.29 | 353.12 ± 12.08 |
| tau b-veto | 71.16 ± 3.34 | 889.44 ± 23.20 | 242.24 ± 10.22 | 348.66 ± 12.05 |
| $MET > 20$ | 67.65 ± 3.31 | 794.96 ± 22.17 | 225.27 ± 10.04 | 260.70 ± 10.75 |

|  | $Z \rightarrow \tau\tau$ | Rare | $t\bar{t}$ | $t\bar{t}V$ |
|---|---|---|---|---|
| this region | 925.53 ± 13.61 | 1663.66 ± 14.18 | 38147.40 ± 70.73 | 280.98 ± 2.22 |
| tau b-veto | 890.47 ± 13.41 | 1597.53 ± 13.90 | 36357.61 ± 69.09 | 269.13 ± 2.17 |
| $MET > 20$ | 790.93 ± 12.29 | 1505.94 ± 13.51 | 34106.16 ± 66.92 | 255.26 ± 2.12 |

|  | $\bar{t}t \rightarrow bWcH$ | $cg \rightarrow tH$ | tcH merged signal | $\bar{t}t \rightarrow bWuH$ |
|---|---|---|---|---|
| this region | 143.63 ± 1.20 | 4.69 ± 0.07 | 148.32 ± 1.21 | 150.75 ± 1.19 |
| tau b-veto | 138.88 ± 1.18 | 4.55 ± 0.07 | 143.44 ± 1.19 | 145.97 ± 1.18 |
| $MET > 20$ | 124.63 ± 1.12 | 4.19 ± 0.07 | 128.82 ± 1.12 | 130.45 ± 1.11 |

|  | $ug \rightarrow tH$ | tuH merged signal | Data |
|---|---|---|---|
| this region | 25.91 ± 0.40 | 176.67 ± 1.26 | 40510.00 ± 201.27 |
| tau b-veto | 25.18 ± 0.39 | 171.15 ± 1.24 | 38568.00 ± 196.39 |
| $MET > 20$ | 23.45 ± 0.38 | 153.90 ± 1.17 | 36026.00 ± 189.81 |

Table 12: cutflow TTH $\tau_{\text{lep}}\tau_{\text{had}}$ ss

|  | SM Higgs | W+jets | Diboson | $Z \rightarrow ll$ |
|---|---|---|---|---|
| this region | 26.72 ± 0.90 | 567.04 ± 19.02 | 88.17 ± 7.79 | 106.42 ± 7.41 |
| tau b-veto | 25.39 ± 0.90 | 550.88 ± 18.75 | 84.88 ± 7.70 | 103.57 ± 7.40 |
| $MET > 20$ | 24.20 ± 0.90 | 487.57 ± 17.44 | 77.40 ± 7.39 | 79.88 ± 6.82 |

|  | $Z \rightarrow \tau\tau$ | Rare | $t\bar{t}$ | $t\bar{t}V$ |
|---|---|---|---|---|
| this region | 20.68 ± 3.52 | 255.43 ± 5.42 | 5900.93 ± 27.81 | 120.64 ± 1.21 |
| tau b-veto | 19.80 ± 3.51 | 231.52 ± 5.16 | 5074.96 ± 25.86 | 114.68 ± 1.17 |
| $MET > 20$ | 17.28 ± 3.29 | 210.21 ± 4.90 | 4659.55 ± 24.78 | 108.49 ± 1.14 |

|  | $\bar{t}t \rightarrow bWcH$ | $cg \rightarrow tH$ | tcH merged signal | $\bar{t}t \rightarrow bWuH$ |
|---|---|---|---|---|
| this region | 45.49 ± 0.53 | 0.77 ± 0.03 | 46.26 ± 0.53 | 49.55 ± 0.55 |
| tau b-veto | 44.09 ± 0.52 | 0.75 ± 0.02 | 44.84 ± 0.52 | 48.05 ± 0.54 |
| $MET > 20$ | 41.16 ± 0.50 | 0.70 ± 0.02 | 41.86 ± 0.50 | 44.55 ± 0.52 |

|  | $ug \rightarrow tH$ | tuH merged signal | Data |
|---|---|---|---|
| this region | 4.72 ± 0.14 | 54.26 ± 0.57 | 7284.00 ± 85.35 |
| tau b-veto | 4.57 ± 0.14 | 52.62 ± 0.56 | 6467.00 ± 80.42 |
| $MET > 20$ | 4.33 ± 0.14 | 48.89 ± 0.54 | 5783.00 ± 76.05 |

Table 13: cutflow $l\tau_{\text{had}}\tau_{\text{had}}$ os

|  | SM Higgs | W+jets | Diboson | $Z \to ll$ |
|---|---|---|---|---|
| this region | $10.67 \pm 0.52$ | $36.63 \pm 13.92$ | $16.76 \pm 1.31$ | $15.46 \pm 6.68$ |
| tau b-veto | $9.99 \pm 0.52$ | $35.74 \pm 13.91$ | $15.70 \pm 1.30$ | $14.14 \pm 6.58$ |

|  | $Z \to \tau\tau$ | Rare | $t\bar{t}$ | $t\bar{t}V$ |
|---|---|---|---|---|
| this region | $19.37 \pm 4.62$ | $24.60 \pm 1.49$ | $341.34 \pm 6.68$ | $18.99 \pm 0.42$ |
| tau b-veto | $18.06 \pm 4.58$ | $22.45 \pm 1.42$ | $269.52 \pm 5.97$ | $17.59 \pm 0.40$ |

|  | $\bar{t}t \to bWcH$ | $cg \to tH$ | tcH merged signal | $\bar{t}t \to bWuH$ |
|---|---|---|---|---|
| this region | $66.70 \pm 0.63$ | $5.10 \pm 0.06$ | $71.80 \pm 0.64$ | $68.95 \pm 0.65$ |
| tau b-veto | $62.40 \pm 0.61$ | $4.79 \pm 0.06$ | $67.19 \pm 0.62$ | $64.88 \pm 0.63$ |

|  | $ug \to tH$ | tuH merged signal | Data |
|---|---|---|---|
| this region | $23.74 \pm 0.30$ | $92.69 \pm 0.71$ | $441.00 \pm 21.00$ |
| tau b-veto | $22.46 \pm 0.29$ | $87.34 \pm 0.69$ | $350.00 \pm 18.71$ |

Table 14: cutflow $l\tau_{\text{had}}\tau_{\text{had}}$ ss

|  | SM Higgs | W+jets | Diboson | $Z \to ll$ |
|---|---|---|---|---|
| this region | $1.66 \pm 0.04$ | $-0.90 \pm 14.73$ | $3.55 \pm 0.70$ | $13.57 \pm 4.40$ |
| tau b-veto | $1.53 \pm 0.04$ | $-1.05 \pm 14.73$ | $3.30 \pm 0.70$ | $13.29 \pm 4.39$ |

|  | $Z \to \tau\tau$ | Rare | $t\bar{t}$ | $t\bar{t}V$ |
|---|---|---|---|---|
| this region | $15.91 \pm 3.36$ | $28.71 \pm 1.84$ | $382.91 \pm 7.07$ | $5.11 \pm 0.23$ |
| tau b-veto | $14.46 \pm 3.32$ | $24.90 \pm 1.71$ | $300.95 \pm 6.29$ | $4.62 \pm 0.22$ |

|  | $\bar{t}t \to bWcH$ | $cg \to tH$ | tcH merged signal | $\bar{t}t \to bWuH$ |
|---|---|---|---|---|
| this region | $4.91 \pm 0.19$ | $0.31 \pm 0.02$ | $5.22 \pm 0.19$ | $5.89 \pm 0.21$ |
| tau b-veto | $4.58 \pm 0.18$ | $0.28 \pm 0.02$ | $4.86 \pm 0.18$ | $5.50 \pm 0.20$ |

|  | $ug \to tH$ | tuH merged signal | Data |
|---|---|---|---|
| this region | $1.69 \pm 0.09$ | $7.58 \pm 0.22$ | $352.00 \pm 18.76$ |
| tau b-veto | $1.57 \pm 0.08$ | $7.08 \pm 0.22$ | $289.00 \pm 17.00$ |

Table 15: cutflow 2lSS $\tau_{\text{had}}$ os

|  | SM Higgs | W+jets | Diboson | $Z \to ll$ |
|---|---|---|---|---|
| this region | $1.91 \pm 0.05$ | $0.28 \pm 0.28$ | $2.08 \pm 0.20$ | $0.01 \pm 0.01$ |
| tau b-veto | $1.85 \pm 0.05$ | $0.28 \pm 0.28$ | $2.05 \pm 0.19$ | $0.01 \pm 0.01$ |

|  | $Z \to \tau\tau$ | Rare | $t\bar{t}$ | $t\bar{t}V$ |
|---|---|---|---|---|
| this region | $0.22 \pm 0.13$ | $1.97 \pm 0.26$ | $11.04 \pm 1.17$ | $7.33 \pm 0.23$ |
| tau b-veto | $0.22 \pm 0.13$ | $1.93 \pm 0.26$ | $10.81 \pm 1.16$ | $7.08 \pm 0.23$ |

|  | $\bar{t}t \to bWcH$ | $cg \to tH$ | tcH merged signal | $\bar{t}t \to bWuH$ |
|---|---|---|---|---|
| this region | $8.89 \pm 0.23$ | $0.62 \pm 0.02$ | $9.51 \pm 0.23$ | $9.01 \pm 0.23$ |
| tau b-veto | $8.67 \pm 0.22$ | $0.61 \pm 0.02$ | $9.28 \pm 0.23$ | $8.72 \pm 0.23$ |

|  | $ug \to tH$ | tuH merged signal | Data |
|---|---|---|---|
| this region | $3.11 \pm 0.11$ | $12.12 \pm 0.25$ | $26.00 \pm 5.10$ |
| tau b-veto | $3.02 \pm 0.11$ | $11.75 \pm 0.25$ | $23.00 \pm 4.80$ |

Table 16: The sample and data yield before the fit.

| | $l\tau_{\mathrm{had}}\tau_{\mathrm{had}}$ ss | $l\tau_{\mathrm{had}}\tau_{\mathrm{had}}$ os | STH $\tau_{\mathrm{lep}}\tau_{\mathrm{had}}$ ss | STH $\tau_{\mathrm{lep}}\tau_{\mathrm{had}}$ os |
|---|---|---|---|---|
| data | $289.00 \pm 17.00$ | $350.00 \pm 18.71$ | $5434.00 \pm 73.72$ | $50560.00 \pm 224.86$ |
| background | $359.83 \pm 17.03$ | $401.07 \pm 16.83$ | $5204.37 \pm 45.86$ | $52663.38 \pm 99.84$ |
| $\bar{t}t \to bWcH$ | $3.89 \pm 0.16$ | $61.83 \pm 0.61$ | $49.15 \pm 0.54$ | $95.69 \pm 0.91$ |
| $cg \to tH$ | $0.23 \pm 0.01$ | $4.76 \pm 0.06$ | $1.28 \pm 0.03$ | $5.25 \pm 0.07$ |
| tcH merged signal | $4.12 \pm 0.16$ | $66.58 \pm 0.61$ | $50.44 \pm 0.54$ | $100.95 \pm 0.91$ |
| $\bar{t}t \to bWuH$ | $4.89 \pm 0.18$ | $64.09 \pm 0.62$ | $51.44 \pm 0.56$ | $98.32 \pm 0.90$ |
| $ug \to tH$ | $1.27 \pm 0.07$ | $22.23 \pm 0.29$ | $7.06 \pm 0.16$ | $26.89 \pm 0.38$ |
| tuH merged signal | $6.16 \pm 0.19$ | $86.32 \pm 0.69$ | $58.51 \pm 0.58$ | $125.21 \pm 0.98$ |

| | TTH $\tau_{\mathrm{lep}}\tau_{\mathrm{had}}$ ss | TTH $\tau_{\mathrm{lep}}\tau_{\mathrm{had}}$ os | $l\tau_{\mathrm{had}}\tau_{\mathrm{had}}$ 2b ss | $l\tau_{\mathrm{had}}\tau_{\mathrm{had}}$ 2b os |
|---|---|---|---|---|
| data | $5783.00 \pm 76.05$ | $36026.00 \pm 189.81$ | $114.00 \pm 10.68$ | $151.00 \pm 12.29$ |
| background | $5664.91 \pm 32.48$ | $38004.97 \pm 74.38$ | $138.65 \pm 4.16$ | $129.13 \pm 3.87$ |
| $\bar{t}t \to bWcH$ | $40.49 \pm 0.49$ | $123.79 \pm 1.11$ | $0.34 \pm 0.05$ | $5.30 \pm 0.18$ |
| $cg \to tH$ | $0.69 \pm 0.02$ | $4.17 \pm 0.07$ | $0.01 \pm 0.00$ | $0.13 \pm 0.01$ |
| tcH merged signal | $41.18 \pm 0.49$ | $127.96 \pm 1.11$ | $0.35 \pm 0.05$ | $5.43 \pm 0.18$ |
| $\bar{t}t \to bWuH$ | $43.74 \pm 0.51$ | $129.80 \pm 1.10$ | $0.06 \pm 0.02$ | $1.28 \pm 0.09$ |
| $ug \to tH$ | $4.27 \pm 0.13$ | $23.39 \pm 0.38$ | $0.02 \pm 0.01$ | $0.36 \pm 0.04$ |
| tuH merged signal | $48.01 \pm 0.53$ | $153.20 \pm 1.17$ | $0.08 \pm 0.02$ | $1.64 \pm 0.10$ |

| | STH $\tau_{\mathrm{lep}}\tau_{\mathrm{had}}$ 2b ss | STH $\tau_{\mathrm{lep}}\tau_{\mathrm{had}}$ 2b os | TTH $\tau_{\mathrm{lep}}\tau_{\mathrm{had}}$ 2b ss | TTH $\tau_{\mathrm{lep}}\tau_{\mathrm{had}}$ 2b os |
|---|---|---|---|---|
| data | $1872.00 \pm 43.27$ | $19549.00 \pm 139.82$ | $1783.00 \pm 42.23$ | $11708.00 \pm 108.20$ |
| background | $1892.90 \pm 15.47$ | $20701.91 \pm 51.56$ | $1738.33 \pm 14.61$ | $12418.20 \pm 39.52$ |
| $\bar{t}t \to bWcH$ | $4.19 \pm 0.16$ | $10.37 \pm 0.32$ | $3.13 \pm 0.14$ | $10.19 \pm 0.32$ |
| $cg \to tH$ | $0.05 \pm 0.01$ | $0.28 \pm 0.02$ | $0.04 \pm 0.01$ | $0.16 \pm 0.01$ |
| tcH merged signal | $4.24 \pm 0.16$ | $10.64 \pm 0.32$ | $3.17 \pm 0.14$ | $10.36 \pm 0.32$ |
| $\bar{t}t \to bWuH$ | $1.94 \pm 0.11$ | $4.96 \pm 0.21$ | $1.69 \pm 0.10$ | $5.47 \pm 0.23$ |
| $ug \to tH$ | $0.26 \pm 0.03$ | $1.22 \pm 0.08$ | $0.17 \pm 0.03$ | $0.87 \pm 0.08$ |
| tuH merged signal | $2.21 \pm 0.11$ | $6.18 \pm 0.22$ | $1.86 \pm 0.10$ | $6.34 \pm 0.24$ |

Table 17: The sample and data yield before the fit.

| | $2lSS\tau_{\mathrm{had}}$ os | $2lSS\tau_{\mathrm{had}}$ os antiiso | $2lSS\tau_{\mathrm{had}}$ os antiisolead |
|---|---|---|---|
| data | $23.00 \pm 4.80$ | $66.00 \pm 8.12$ | $19.00 \pm 4.36$ |
| background | $23.48 \pm 1.21$ | $70.26 \pm 2.98$ | $22.93 \pm 1.74$ |
| $\bar{t}t \to bWcH$ | $8.66 \pm 0.22$ | $2.17 \pm 0.11$ | $0.81 \pm 0.07$ |
| $cg \to tH$ | $0.61 \pm 0.02$ | $0.15 \pm 0.01$ | $0.04 \pm 0.01$ |
| tcH merged signal | $9.27 \pm 0.22$ | $2.32 \pm 0.11$ | $0.86 \pm 0.07$ |
| $\bar{t}t \to bWuH$ | $8.71 \pm 0.23$ | $2.33 \pm 0.12$ | $0.81 \pm 0.07$ |
| $ug \to tH$ | $3.02 \pm 0.11$ | $0.77 \pm 0.05$ | $0.27 \pm 0.03$ |
| tuH merged signal | $11.73 \pm 0.25$ | $3.10 \pm 0.13$ | $1.07 \pm 0.08$ |

Table 18: The stat. only significance of the signal in each regions with the benchmark $\mu$ value.

| | $l\tau_{\text{had}}\tau_{\text{had}}$ ss | $l\tau_{\text{had}}\tau_{\text{had}}$ os | STH $\tau_{\text{lep}}\tau_{\text{had}}$ ss | STH $\tau_{\text{lep}}\tau_{\text{had}}$ os |
|---|---|---|---|---|
| $\bar{t}t \to bWcH$ | 0.22 | 5.83 | 0.80 | 0.84 |
| $cg \to tH$ | 0.01 | 0.55 | 0.02 | 0.09 |
| tcH merged signal | 0.23 | 6.23 | 0.82 | 0.92 |
| $\bar{t}t \to bWuH$ | 0.28 | 6.21 | 0.84 | 0.84 |
| $ug \to tH$ | 0.07 | 2.37 | 0.11 | 0.55 |
| tuH merged signal | 0.34 | 7.99 | 0.96 | 1.34 |

| | TTH $\tau_{\text{lep}}\tau_{\text{had}}$ ss | TTH $\tau_{\text{lep}}\tau_{\text{had}}$ os | $l\tau_{\text{had}}\tau_{\text{had}}$ 2b ss | $l\tau_{\text{had}}\tau_{\text{had}}$ 2b os |
|---|---|---|---|---|
| $\bar{t}t \to bWcH$ | 0.59 | 1.89 | 0.03 | 0.99 |
| $cg \to tH$ | 0.01 | 0.08 | 0.00 | 0.02 |
| tcH merged signal | 0.60 | 1.97 | 0.03 | 1.01 |
| $\bar{t}t \to bWuH$ | 0.64 | 1.98 | 0.01 | 0.25 |
| $ug \to tH$ | 0.07 | 0.47 | 0.00 | 0.07 |
| tuH merged signal | 0.71 | 2.43 | 0.01 | 0.32 |

| | STH $\tau_{\text{lep}}\tau_{\text{had}}$ 2b ss | STH $\tau_{\text{lep}}\tau_{\text{had}}$ 2b os | TTH $\tau_{\text{lep}}\tau_{\text{had}}$ 2b ss | TTH $\tau_{\text{lep}}\tau_{\text{had}}$ 2b os |
|---|---|---|---|---|
| $\bar{t}t \to bWcH$ | 0.12 | 0.20 | 0.08 | 0.27 |
| $cg \to tH$ | 0.00 | 0.01 | 0.00 | 0.00 |
| tcH merged signal | 0.12 | 0.20 | 0.09 | 0.27 |
| $\bar{t}t \to bWuH$ | 0.05 | 0.09 | 0.05 | 0.13 |
| $ug \to tH$ | 0.01 | 0.05 | 0.01 | 0.03 |
| tuH merged signal | 0.06 | 0.13 | 0.05 | 0.16 |

Table 19: The stat. only significance of the signal in each regions with the benchmark $\mu$ value.

| | $2lSS\tau_{\text{had}}$ os | $2lSS\tau_{\text{had}}$ os antiiso | $2lSS\tau_{\text{had}}$ os antiisolead |
|---|---|---|---|
| $\bar{t}t \to bWcH$ | 1.72 | 0.26 | 0.19 |
| $cg \to tH$ | 0.21 | 0.04 | 0.04 |
| tcH merged signal | 1.83 | 0.28 | 0.22 |
| $\bar{t}t \to bWuH$ | 1.89 | 0.35 | 0.28 |
| $ug \to tH$ | 1.05 | 0.19 | 0.15 |
| tuH merged signal | 2.70 | 0.52 | 0.40 |

# 7 FCNC signal samples

The targeted signal in this analysis is $tqH/tH$ with $H \rightarrow \tau\tau$ (samples 411170-411177 and 412098-412105) in App. **??**). However, if the FCNC processes exists, the other decays of the Higgs can be part of the signal. Therefore, samples xxxxxx-xxxxxx (App. **??**) with inclusive $W$ and Higgs decays are also included. These sample have a one-lepton (electron or muon) filter at truth level (either coming from $W$ or Higgs decays). Events overlapping with 410818-410839 are removed based on truth information.

It is checked that after the final selection, there are 110 overlapped signal events caused by different overlap removal and object definition in xTauFramework and ttHMultiAna (27140 in total for hadhad channel and 95253 in total for lepton channels) but there is no overlap in the signal enriched region (BDT > 0.5).

The total FCNC signal with fake taus in this analysis is not used in the MVA training, but is regarded as part of the total signal in the fit. The normalization factor of the other components is common with the signal, so that their yields are fully correlated in the fit. In Sec. **??**, this signal is summed with the nominal signal in the control plots. The signal fake tau shares the same normalisation and systematics as described in **??**.

# 8 Background estimation

The background events with real tau leptons are represented by Monte Carlo (MC) samples. These include $t\bar{t}$, $t\bar{t}+H/V$ and single top events with real taus, and $Z \rightarrow \tau\tau$+jets. The $Z \rightarrow ee, \mu\mu$ processes are included for lepton faking tau background, and the contribution from jet faking tau. The fake background with one or more taus faked by jets consists of the top fake (with at least one fake tau from jets in the top events), QCD multijet, $W$+jets and diboson events. Since a jet can be reconstructed as a fake tau with equal probability charge being positive or negative at the first order, the fake taus in the opposite-sign di-tau events could be estimated using the same-sign events after correction of the truth tau contributions. However, the charge of two taus candidates might be correlated in the $t\bar{t}$ events when one of taus is a real tau from the $W \rightarrow \tau\nu$ decay while the other tau is a fake from a jet from other $W \rightarrow jj$ decay. They are likely to carry the opposite charges to each other. Because of this charge asymmetry we have to calibrate the fake-tau modeling using a Data-Driven (DD) Scale Factor (SF) method by comparing the normalization of fake-tau events in MC to data in the dilepton + jets control regions. This SF is then applied to correct the normalization of tau fakes in the MC yields. The excess of the SS events over these MC background in $\tau_{\text{had}}\tau_{\text{had}}$ is dominated by the fake-tau background from multi-jets (QCD). However, for the leptonic events, the fake-tau contribution is dominated by the $t\bar{t}$ events and we simply estimate the fake-tau background by correcting the normalization of tau fakes in the MC yields.

## 8.1 Origin of fake $\tau_{had}$

Top fake is the largest fake background in the total fake in the leptonic channels. Within the top fake events, fake taus can come from different origins, i.e., from jets (heavy/light flavor quark or gluon initiated) or leptons (electron or muon). Different fake origins in SS and OS can induce additional systematics. To this end, the tau fake origins are checked with the top MC. Three dedicated top pair production control regions are define for:

- W-jet faking tau: exactly 1 lepton, exactly 1 tau candidate, exactly 3 jets with exactly 2 b-tagged. Tau candidate and lepton have the same charge.

- B-jet faking tau: 2 leptons with different flavors or away from Z pole ($M_{ll} > 100$GeV or $M_{ll} < 90$GeV), exactly 1 tau candidate, exactly 1 b-tagged jet.

- Radiation faking tau: 2 leptons with different flavors or away from Z pole, exactly 1 tau candidate, exactly 2 b-tagged jets.

Figure 5 shows the fractions of fake taus from different origins in top control regions and SS, OS signal regions. The matching between tau candidates and truth particles or partons are based on $\Delta R < 0.4$. Most of the fake taus come from quark initiated jets, but the flavor distributions in OS are similar to those in SS.

## 8.2 MC fake $\tau_{had}$ estimation (obsolete)

To estimate the fake tau background from MC, we use the same Data-Driven (DD) Scale Factor (SF) method developed for the ATLAS ttH multi-lepton analysis [**ATL-COM-PHYS-2018-410**] in which the SF is derived in the opposite-sign dilepton + $\tau_{had}$ ($2lOS+1\tau_{had}$) control region by comparing the rate of observed fake-tau events to the MC simulation. The scale factors are parametrized as a function of $p_T$ for 1- and 3-prong $\tau_{had}$ separately and the final SF are summarized in Table 19. The systematics on the scale factors are derived by comparing the values in the nominal control region to those obtained in either enriched $t\bar{t}$ or $Z$ boson control regions respectively.

Table 20: The fake-tau SF measured from the control regions as a function of tau $p_T$ where uncertainty is divided into statistical and systematic obtained from control regions enriched in $t\bar{t}$ and $Z$ + jets. The $p_T$ bins for 1-prong(3-prong) $\tau_{had}$ are listed separately.

| type of $\tau_{had}$ | 25-45(25-50) GeV | 45-70(50-75) GeV | > 70(75) GeV |
|---|---|---|---|
| 1-prong | 1.05±0.04±0.05 | 0.94±0.08±0.21 | 0.64±0.10±0.07 |
| 3-prong | 1.25±0.10±0.41 | 1.30±0.32±0.72 | 0.52±0.30±0.64 |

These SF are then applied to correct the normalization of MC yields in the for both leptonic and hadronic channels. To validate the fake-tau estimate, we have compared the leading $\tau_{\text{had}}$ $p_{\text{T}}$ between data and MC prediction using the events in the same-sign control region where the di-tau have the same-sign charge (SS). The distributions are shown in Figure **??**. The data are in good agreement with MC predictions, which indicated the fake tau is well modeled in MC.

## 8.3 MC fake $\tau_{\text{had}}$ estimation

Although the method mentioned in the 8.2 was adopted by the tthML analysis, a new method is needed in this case. As shown in the Figure 6, the data is generally over-estimated in the OS regions while it is opposite in the SS region. If the fake taus are corrected by the same scale factors, this mismodelling will never get solved. This asymmetry of the SS and OS fake taus can be interpreted by the mis-modelling of the fake tau charges. Since the fake taus mainly come from light-flavored jets as shown in Figure 5, the mis-modelling is related to the charge carried by the jets. In conclusion, the mis-modelling is originated from the charge correlation between the jet which is faking a tau and the lepton. So the parent of the jet is believed to be charge correlated with the lepton. Considering the main background is $\bar{t}t$ process. The only suspect is the hadronic $W$ boson. In order to find the contribution of w-jet faking taus ($\tau_W$). the truth information is used to match between the w-jet and the fake tau with $\Delta R < 0.2$. As shown in the Figure 7, there is a considerable amount of $\tau_W$'s in both SS and OS regions. There are three kinds of fake taus that need to be calibrated: Type1) $\tau_W$'s with the opposite charge of the lepton; Type2) $\tau_W$'s with the same charge of the lepton; Type3) the fake taus that are not from $W$-decay jets. Many control regions are used to calibrate the three components:

- $2l1tau1b$: 2 leptons with different flavors or away from Z pole, exactly 1 tau candidate, exactly 1 b-tagged jets.

- $2l1tau2b$: 2 leptons with different flavors or away from Z pole, exactly 1 tau candidate, exactly 2 b-tagged jets.

- $1l1tau2b2jSS$: Exactly 1 lepton, exactly 1 tau candidate, exactly 4 jets with exactly 2 b-tagged. Tau candidate and lepton have the same charge.

- $1l1tau2b2jOS$: Exactly 1 lepton, exactly 1 tau candidate, exactly 4 jets with exactly 2 b-tagged. Tau candidate and lepton have the opposite charge.

- $1l1tau2b3jSS$: Exactly 1 lepton, exactly 1 tau candidate, at least 5 jets with exactly 2 b-tagged. Tau candidate and lepton have the same charge.

- $1l1tau2b3jOS$: Exactly 1 lepton, exactly 1 tau candidate, at least 5 jets with exactly 2 b-tagged. Tau candidate and lepton have the opposite charge.

Table 21

|            | $25 - 35$ GeV   | $35 - 45$ GeV   | 45- GeV         |
|------------|-----------------|-----------------|-----------------|
| $\tau_b$   | $0.91 \pm 0.06$ | $1.37 \pm 0.07$ | $1.06 \pm 0.06$ |
| $\tau_{other}$ | $1.26 \pm 0.02$ | $0.92 \pm 0.02$ | $0.92 \pm 0.03$ |
| $\tau_W$   | $0.83 \pm 0.01$ | $0.82 \pm 0.02$ | $0.56 \pm 0.02$ |

Where di-lep regions ($2l1tau1b$ and $2l1tau2b$) are used to calibrate the Type3 fake taus. As explained in the 8.1, these regions are dominated by the bjet and the radiated gluon-jet faking taus. 2bOS regions ($1l1tau2b2jOS$ and $1l1tau2b3jOS$) are used to calibrate Type1 fake taus. Compared to the signal region, this region has an additional b-jet. So the $\bar{t}t$ background is enhanced in this region and signal is depleted. Similarly for the Type2 we can use 2bSS regions ($1l1tau2b2jSS$ and $1l1tau2b3jSS$) to calibrate. The components of these regions are shown in Figure 8. Then two fits are made to derive the scale factors for the fake taus. There are three parameters needed to be decided (the scale factors for the 3 types). But considering the $p_T$ depencence of the tau reconstruction, the scale factors are derived in 3 $p_T$ slices (25-35,35-45,45-inf)GeV. So there are 9 parameters to be decided. Since we only care about the signal region (OS), adding the SS region might worse the modelling, so only the the di-lep regions and 2bOS regions are used. A fit is done to the MC to match the data in these control regions by floating the scale factor of Type1 and Type3 fake taus. The fit result is shown in table **??**. In order to have a cross check, the fit for di-lep and 2bSS regions are also made to derive the scale factor of Type2 and Type3. The results is shown in table **??**. All of the CP and theory uncerntainties are used to derive the uncertainty of the scale factors. It is observed that for both fit, the scale factors of the Type3 fake taus are consistent. The post-fit plots are shown in Figure 9. Then the scale factors are applied to the corresponding single b-jet regions. In $l\tau_{had}\tau_{had}$ channel, both taus can be fake, so the calibration is done to them separately, following the same procedure as $\tau_{lep}\tau_{had}$ channels using the lepton and fake tau charges, then the scale factors are multiplied together. The data-MC comparison is show in Figure 10.

## 8.4 QCD fake $\tau_{had}$ estimate in $\tau_{had}\tau_{had}$

Figure 11 shows the $\tau_{had}$ $p_T$ spectra in the $\tau_{had}\tau_{had}$ SS and OS. The fake tau background events from QCD multi-jets is not added yet so the data have more than the background prediction. The top fake are dominated by fakes with one real tau. It is found, based on the MC prediction, that the QCD fake is the dominant fake process in the $\tau_{had}\tau_{had}$ channel.

The excess of the SS events over MC with truth taus are used to estimate the fake tau background in OS from QCD multi-jets in the $\tau_{had}\tau_{had}$ + jets channel:

$$N_{\text{QCD fake}}^{\text{OS}} = f_{\text{norm}} \cdot (N_{\text{data}}^{\text{SS}} - N_{\text{MC}}^{\text{SS}}), \tag{7}$$

where $f_{\text{norm}}$ is a ratio of OS and SS from multi-jets QCD, $N_{\text{data}}^{\text{SS}}$, and $N_{\text{MC}}^{\text{SS}}$ are observed data and estimated MC predictions in the SS regions.

The $f_{\text{norm}}$ is measured separately to be $1.32 \pm 0.03$ in the signal-depleted one $b$-tag events with $BDT < 0.5$ and $1.6 \pm 0.1$ in the double $b$-tagged $\tau_{\text{had}}\tau_{\text{had}} +\geq 3$jets events, which provides a good closure test of QCD fake tau estimation. We take the difference between these two values as a systematics for the method and assign $f_{\text{norm}} = 1.3 \pm 0.3$ for the analysis.

## 8.5 Fake lepton background

The fake lepton background in $\tau_{\text{lep}}\tau_{\text{had}}$ and lepton+$\tau_{\text{had}}\tau_{\text{had}}$, which is estimated from MC[3], is about 0.3-0.5% of the total background. It constitutes such a negligible fraction because a very high lepton $p_{\text{T}}$ threshold is already required at the trigger level. This background is varied by 100% as a conservative systematics.

## 8.6 Summary of signal and background events

We estimate the expected signal and background events in different regions, which are summarized in Table 23.

Figure 12 shows the leading $\tau_{\text{had}}$ $p_{\text{T}}$ distribution from the OS events in the $\tau_{\text{had}}\tau_{\text{had}}$ signal regions where the points are data and the histograms as the expected various backgrounds.

---

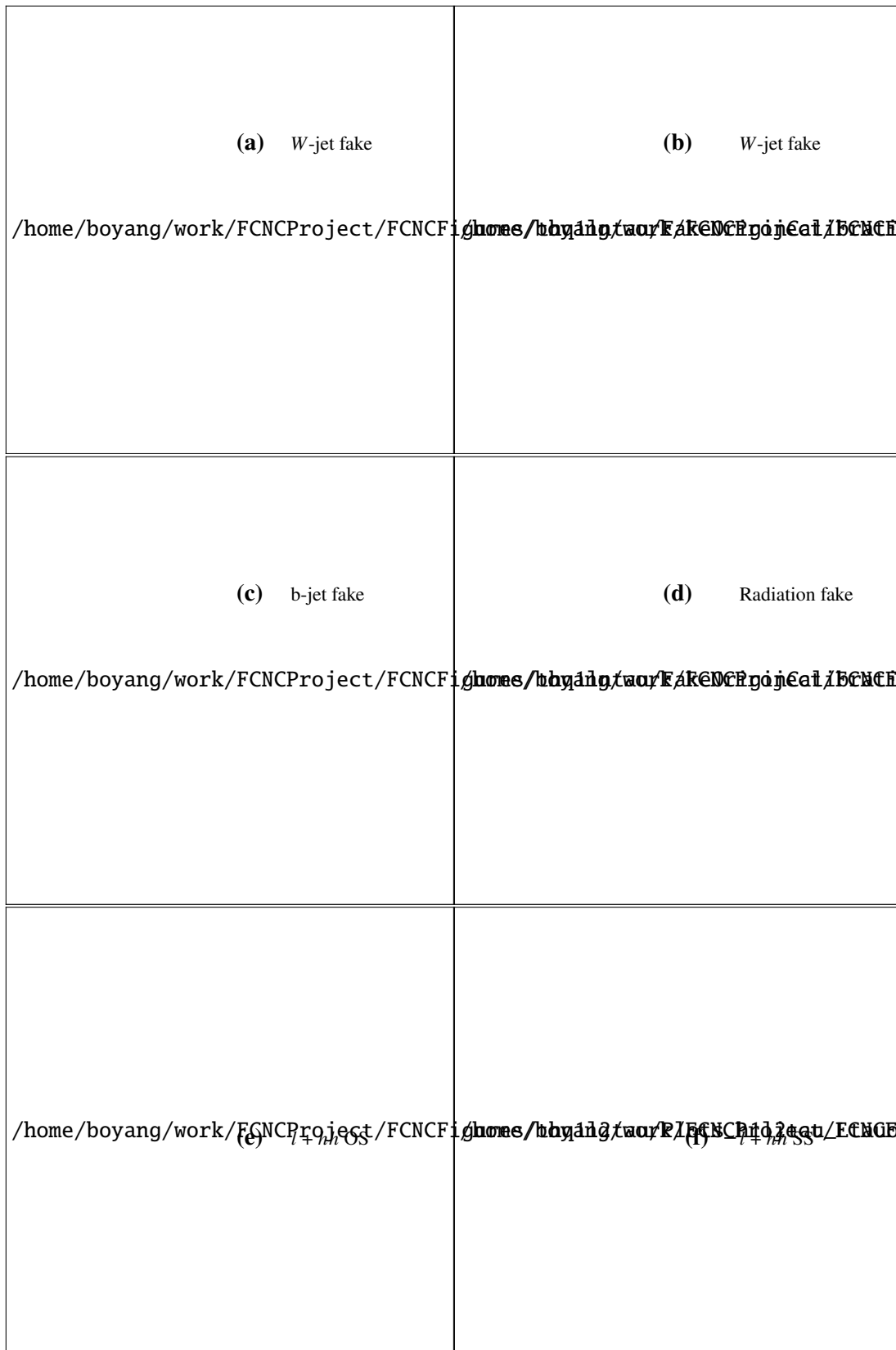[3] This includes fake lepton + real tau events from all MC samples, namely, top, $W/Z$+jets, diboson

**(a)** *W*-jet fake

**(b)** *W*-jet fake

/home/boyang/work/FCNCProject/FCNCFigures/boyang/work/FCNCProject/FCNCFigures/tanpu

**(c)** b-jet fake

**(d)** Radiation fake

/home/boyang/work/FCNCProject/FCNCFigures/boyang/work/FCNCProject/FCNCFigures/tanpu

**(e)** $\tau + \ell_{hh}$ OS

**(f)** $\tau + \ell_{hh}$ SS

/home/boyang/work/FCNCProject/FCNCFigures/boyang/work/FCNCh12tau/FCNCfakes/ibg1h2ga

Figure 5: The origins of fake $\tau$'s in the top fake MC for W-jet fake control region (a,b), b-jet fake control region (c), radiation control region (d); in the leptonic OS (e) and SS (f) categories. The flavor distributions are quite similar between OS and SS.
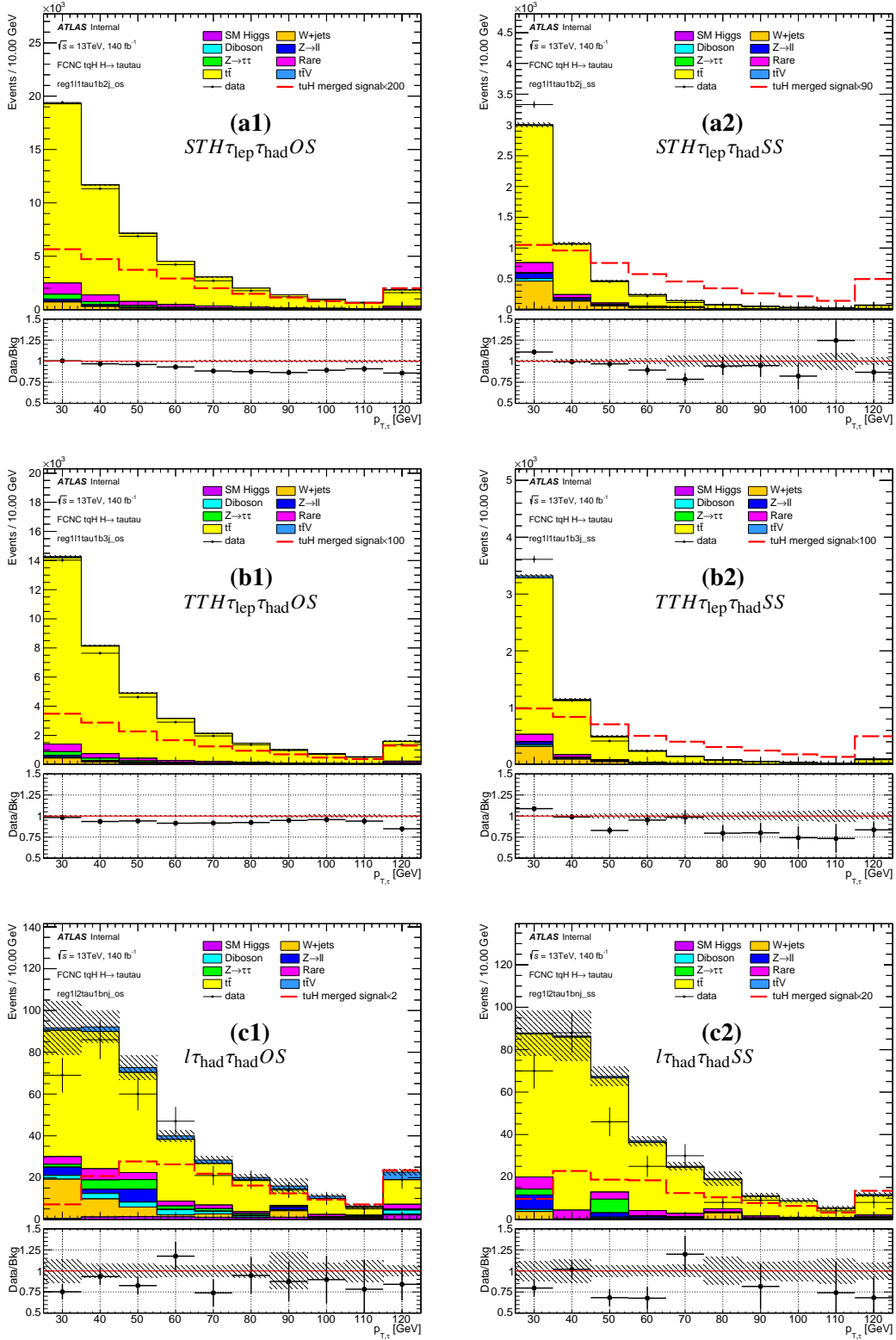
Figure 6: The data-MC comparison of $\tau$ $p_T$ in the signal and SS control regions.
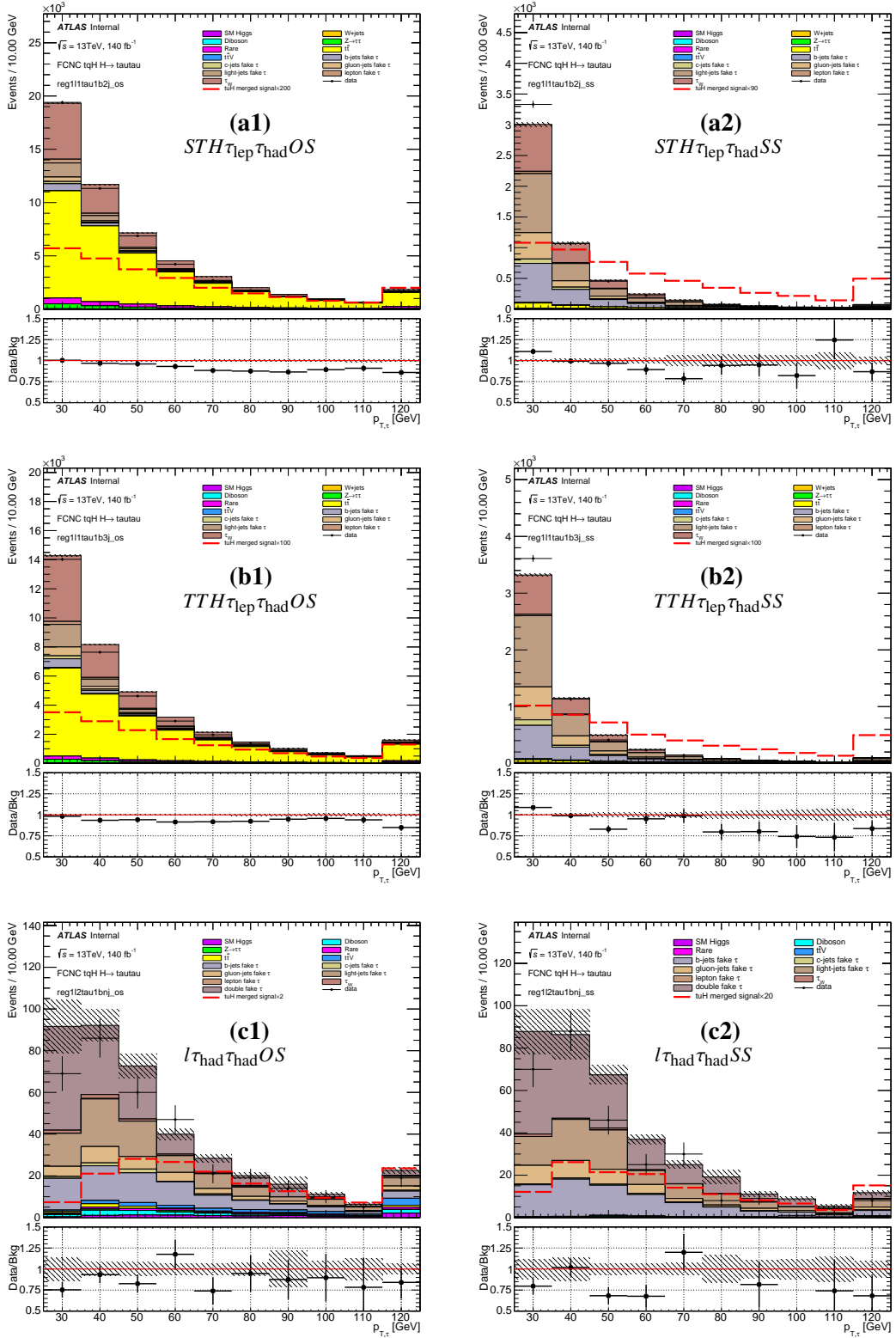
Figure 7: The distributions of $\tau$ $p_{\mathrm{T}}$ in the signal and SS control regions.
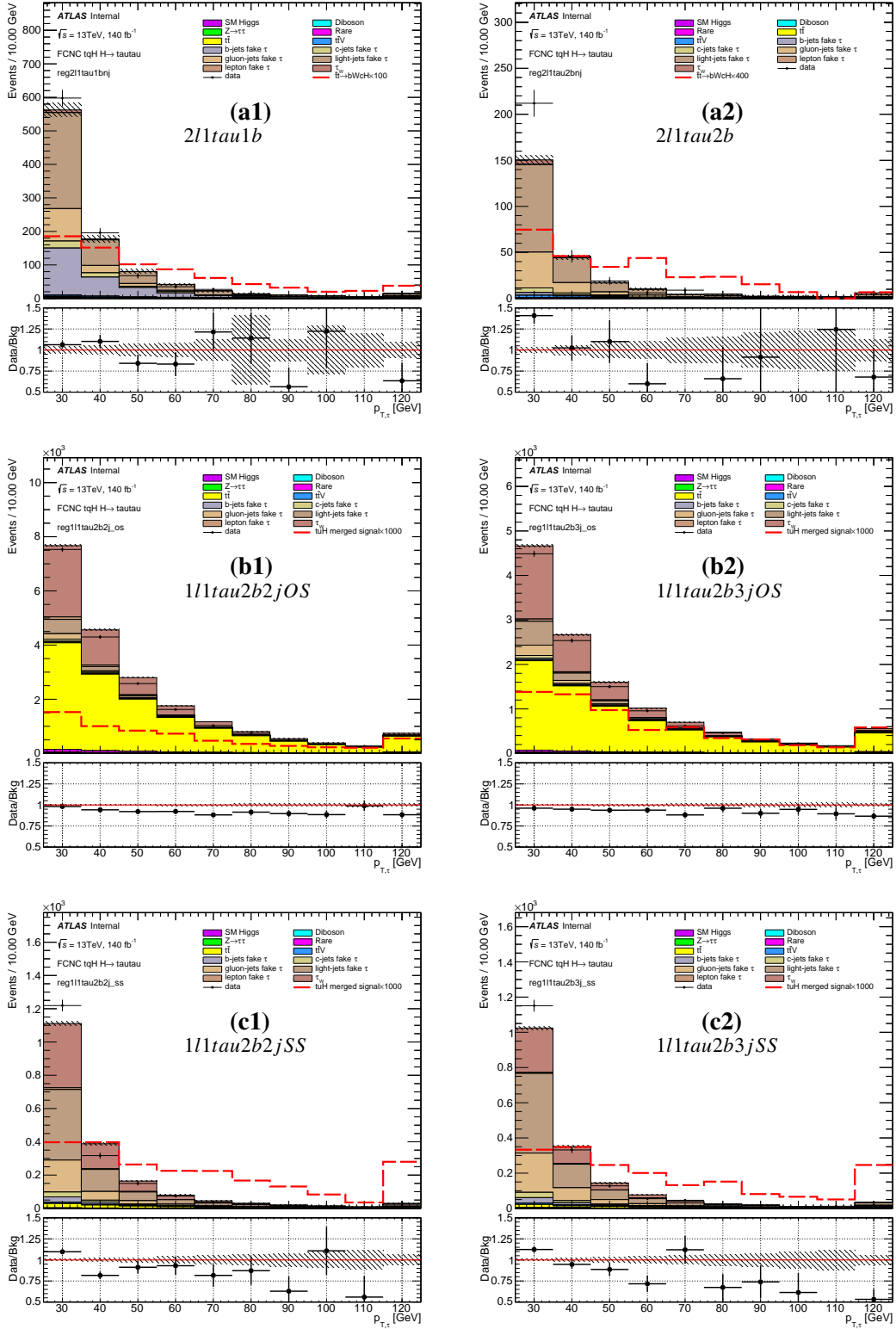
Figure 8: The distributions of $\tau$ $p_T$ in the control regions used to calibrate the fake taus.
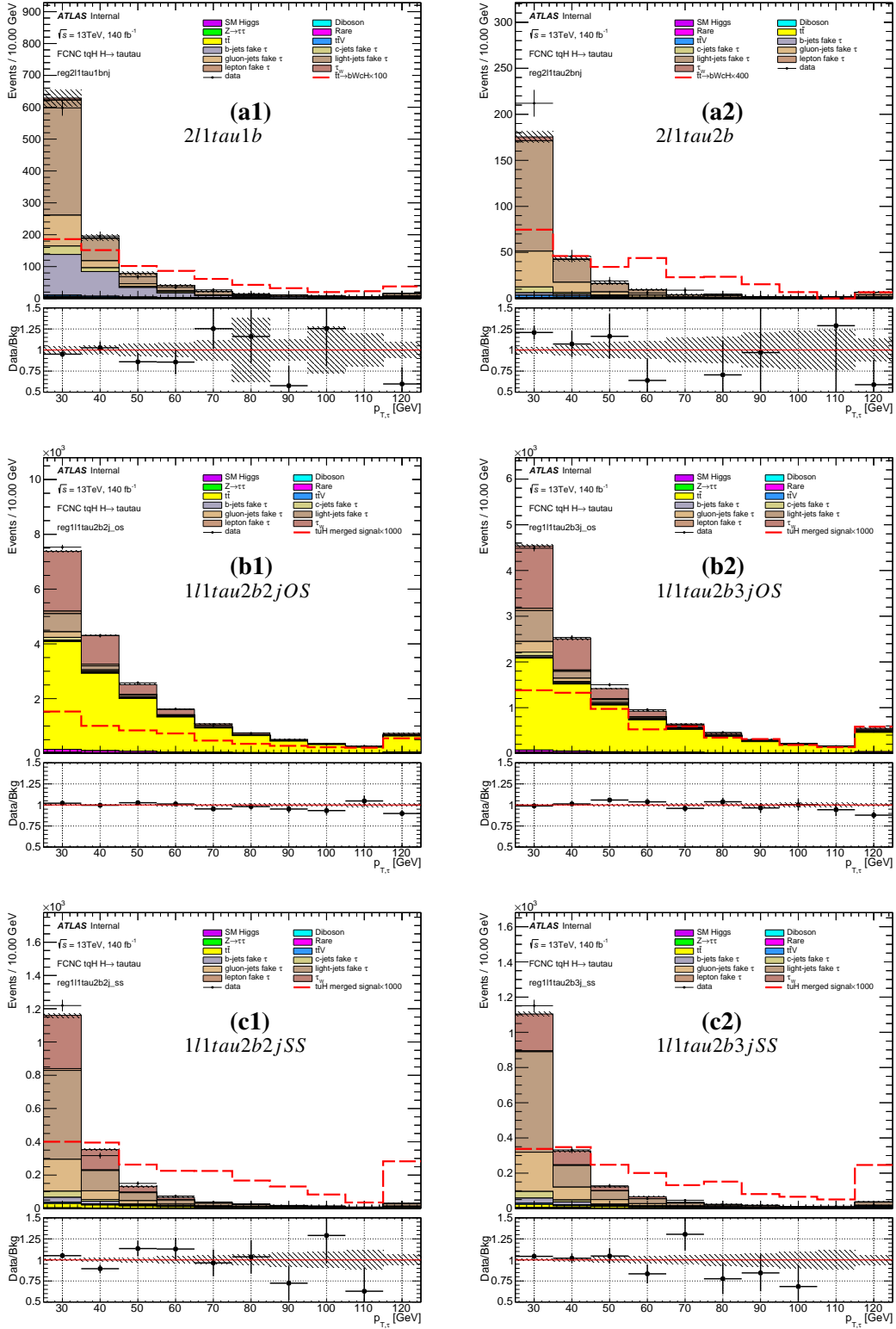
Figure 9: The post-fit distributions of $\tau$ $p_T$ in the control regions after the fake tau correction.
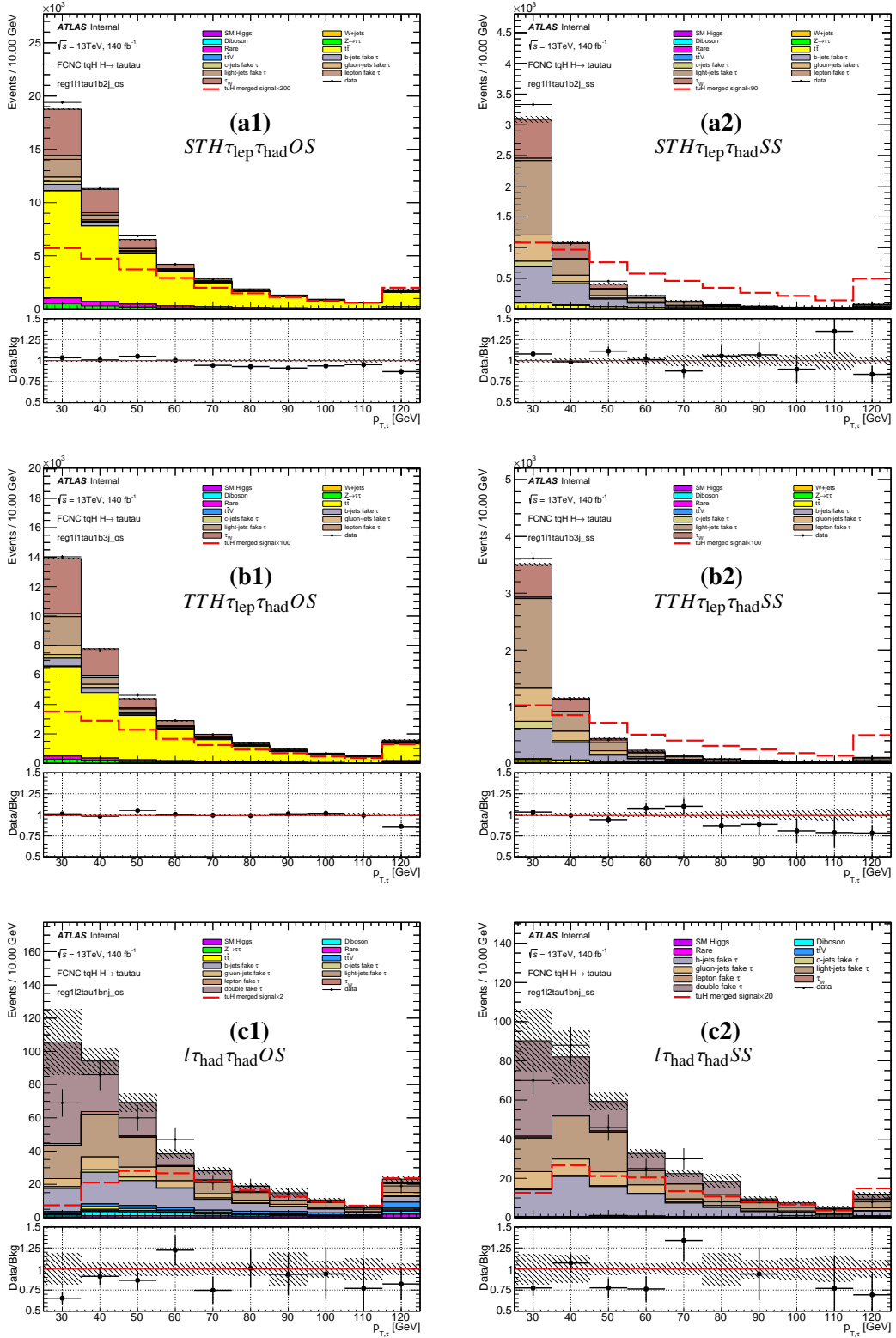
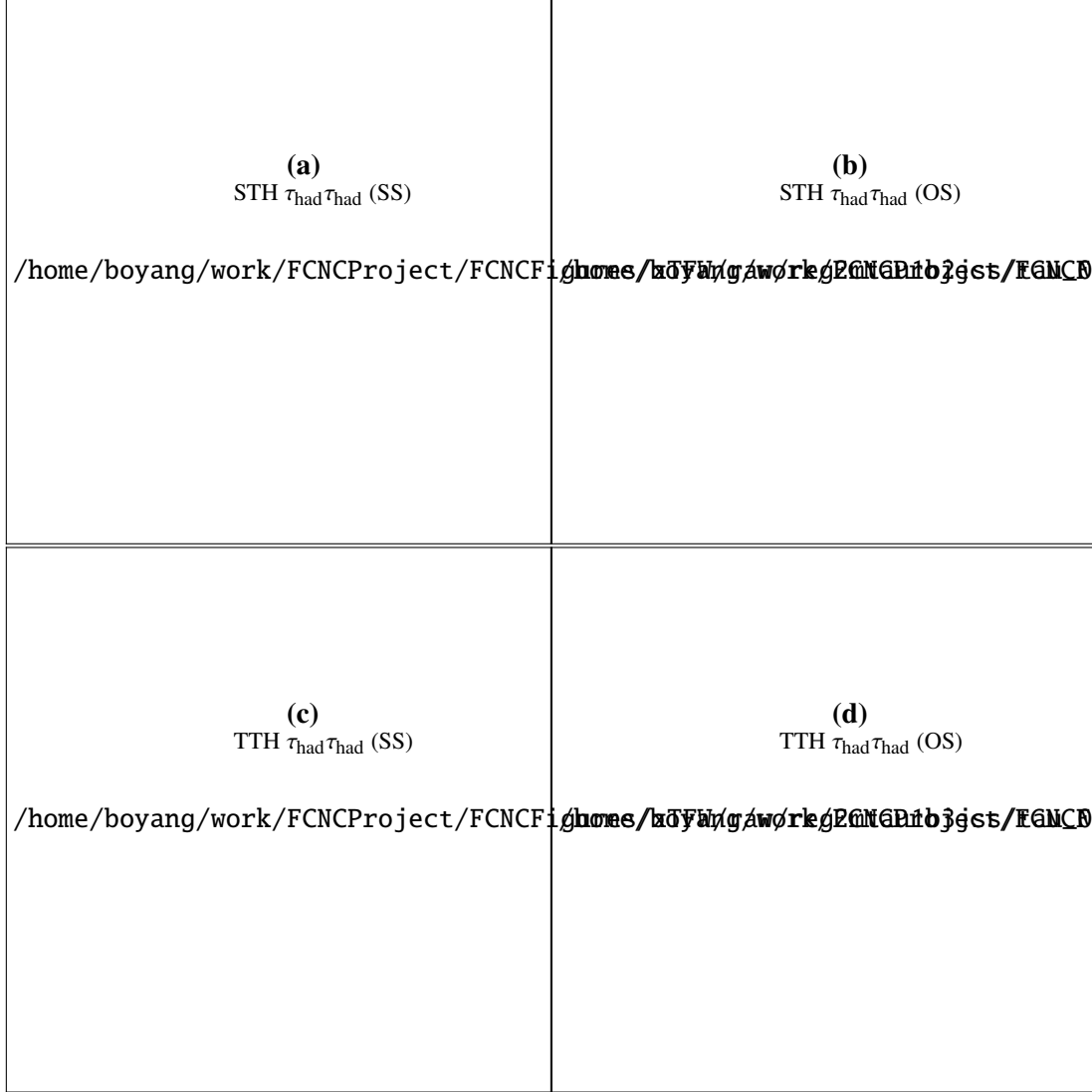Figure 10: The data-MC comparison of $\tau$ $p_{\mathrm{T}}$ in the signal and SS control regions after the fake tau correction.

**(a)**
STH $\tau_{had}\tau_{had}$ (SS)

/home/boyang/work/FCNCProject/FCNCFighomes/boYang/work/PGNGBtb3jest/FGNCPiourpsdfxTFW/raw,

**(b)**
STH $\tau_{had}\tau_{had}$ (OS)

**(c)**
TTH $\tau_{had}\tau_{had}$ (SS)

/home/boyang/work/FCNCProject/FCNCFighomes/boYang/work/PGNGBtb3jest/FGNCPiourpsdfxTFW/raw,

**(d)**
TTH $\tau_{had}\tau_{had}$ (OS)

Figure 11: The distributions of $\tau$ $p_T$ in the STH $\tau_{had}\tau_{had}$ (SS)(a), STH $\tau_{had}\tau_{had}$ (OS) (b), TTH $\tau_{had}\tau_{had}$ (SS) (c) and TTH $\tau_{had}\tau_{had}$ (OS) (d), to illustrate the background composition. Data is more than the prediction because the fake tau backgrounds are missing.
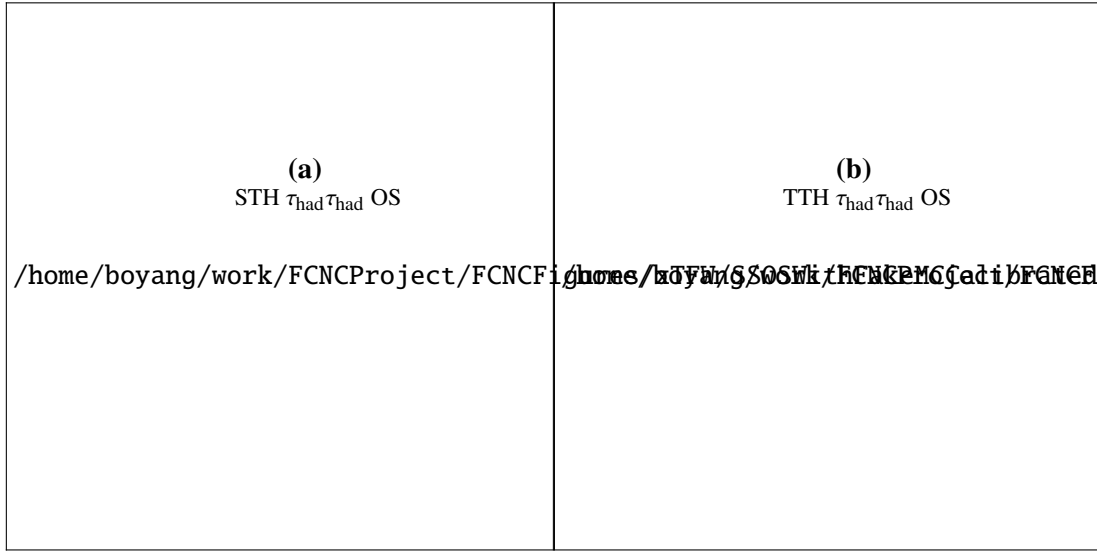
**(a)**
STH $\tau_{\text{had}}\tau_{\text{had}}$ OS

/home/boyang/work/FCNCProject/FCNCFighome/boyang/SwORkithECkeEMCCadti)FGNEFigeg2sxaUHb2JS0S

**(b)**
TTH $\tau_{\text{had}}\tau_{\text{had}}$ OS

Figure 12: The distributions of leading$\tau$ $p_{\text{T}}$ in the $\tau_{\text{had}}\tau_{\text{had}}$ + 3 jets (a), and 4 jets OS (b)

Table 22

| | STH $\tau_{\text{lep}}\tau_{\text{had}}$ OS | TTH $\tau_{\text{lep}}\tau_{\text{had}}$ OS | $l\tau_{\text{had}}\tau_{\text{had}}$ OS | 2lSS $\tau_{\text{had}}$ OS |
|---|---|---|---|---|
| $p_{T,\tau}$ | 9.46 / 9.32 | 9.80 / 8.54 | 6.02 / 9.02 | 4.78 / 5.29 |
| $\Delta R(\tau,\tau)$ | 6.38 / 6.17 | 6.28 / 6.77 | 9.12 / 9.13 | 8.86 / 7.95 |
| $E^T_{miss}$ | 6.56 / 5.72 | 5.62 / 6.08 | 5.62 / 5.24 | 6.87 / 7.39 |
| $m_{\tau\tau,vis}$ | 6.25 / 7.32 | 7.26 / 7.29 | 14.16 / 13.01 | 8.65 / 8.37 |
| $\Delta R(\tau, light\ jet, min)$ | 7.57 / 7.79 | 6.82 / 6.48 | 7.94 / 8.26 | 7.27 / 8.94 |
| $\Delta R(l, b\ jet)$ | 7.53 / 7.31 | 6.99 / 6.01 | 7.05 / 7.39 | 6.36 / 7.38 |
| $\Delta\phi(\tau\tau, P^T_{miss})$ | 5.72 / 6.44 | 5.06 / 5.94 | / | / |
| $E^T_{miss} centrality$ | 5.82 / 5.06 | 4.73 / 4.49 | / | / |
| $m_{\tau,\tau}$ | 10.01 / 10.80 | 11.45 / 11.39 | / | / |
| $m_{t,FCNC}$ | 3.46 / 3.98 | 4.94 / 4.60 | / | / |
| $E_{\nu,1}/E_{\tau,1}$ | 6.46 / 4.76 | 5.74 / 6.08 | / | / |
| $E_{\nu,2}/E_{\tau,2}$ | 7.09 / 6.99 | 5.79 / 5.91 | / | / |
| $m_{t,SM}$ | 5.94 / 6.40 | 6.02 / 5.27 | / | / |
| $\Delta R(\tau, b\ jet)$ | 7.54 / 7.37 | 6.08 / 6.69 | / | / |
| $M(light\ jet, light\ jet, min)$ | 4.19 / 4.58 | 4.89 / 5.40 | / | / |
| $m_W$ | / | 2.54 / 3.07 | / | / |
| $m_{t,SM,vis}$ | / | / | 9.89 / 8.19 | 8.93 / 6.54 |
| $M(\tau\tau light\ jet, min)$ | / | / | 3.74 / 3.13 | 4.51 / 4.89 |
| $\Delta R(l,\tau)$ | / | / | 4.07 / 3.67 | 5.48 / 7.14 |
| $\eta_{\tau,max}$ | / | / | 7.58 / 6.67 | 8.52 / 7.39 |
| $m^T_W$ | / | / | 5.83 / 6.13 | 5.83 / 4.39 |
| $\Delta R(l + b\ jet, \tau + \tau)$ | / | / | 6.52 / 8.00 | 7.69 / 7.21 |
| $P_{t,\tau\tau,vis}$ | / | / | 5.71 / 5.19 | 3.90 / 5.01 |
| $m_{t,FCNC,vis}$ | / | / | 6.75 / 6.96 | 5.95 / 7.37 |
| $p_{T,l}$ | / | / | / | 6.37 / 4.74 |

# 9 MVA analysis

In this section, we investigate the sensitivity of probing signal using one of the Multi-Variate Analysis (MVA) methods, the Gradient Boosted Decision Trees (BDT) method [**BDT**, **BDT2**], with the TMVA software package. The BDT output score is in the range between -1 and 1. The most signal-like events have scores near 1 while the most background-like events have scores near -1.

The signal topology and kinematics are different across all the channels. To maximize the overall sensitivity, separated BDTG trainings are applied to each the signal region. A number of variables as the BDT inputs are used to train and test events in each signal region for maximal signal acceptance and background rejection. They are listed in Tab. **??**.

The signal and background samples are randomly divided into two equal parts (denoted as even and odd parity events). The BDT is trained with one part, and tested on the other part. It is always ensured that the BDT derived from the training events is not applied to the same events, but only to the independent test

ones. The sum of all background processes, corrected normalized, are used in the training and testing. The Gradient BDT parameters used are listed in Tab. **??**. With the `IgnoreNegWeightsInTraining` option, only MC events with positive MC weights are used in the traning. The comparison of BDT performances in test-odd and test-even samples is given in Fig. **??**. The BDT parameters `NTrees` and `nCuts` are tuned such that the test-odd and test-even agrees, and the signal sensitivity is optimised.

The seperation[4] and importance[5] of different variables used in the training are listed in Tab. 21. The last two variables in the importance ranking are moved to check the impact on the MVA performance, and the results can be found in App. **??**.

As a cross check, the comparisons between BDT distributions in testing samples, as well as the test even and test odd ROC curves, are shown in Fig. **??**.

The final yield and stat. only significance is shown in Table 23 and Table 25

---

[4] The separation is defined by, as in [**BDT2**],

$$\langle S^2 \rangle = \frac{1}{2} \int \frac{[p_S(y) - p_B(y)]^2}{p_S(y) + p_B(y)} dy,\tag{8}$$

where $p_S(y)$ and $p_B(y)$ are the signal and background PDFs of the classifier $y$. The separation is 0 (1) for identical (non-overlapping) signal and background shapes.

[5] The importance is evaluated as the total separation gain that this variable had in the decision trees (weighted by the number of events). It is normalized to all variables together, which have an importance of 1.

Table 23: The sample and data yield before the fit.

|  | $l\tau_{\text{had}}\tau_{\text{had}}$ ss | $l\tau_{\text{had}}\tau_{\text{had}}$ os | STH $\tau_{\text{lep}}\tau_{\text{had}}$ ss | STH $\tau_{\text{lep}}\tau_{\text{had}}$ os |
|---|---|---|---|---|
| data | 289.00 ± 17.00 | 350.00 ± 18.71 | 5434.00 ± 73.72 | 50560.00 ± 224.86 |
| background | 339.04 ± 21.91 | 409.73 ± 22.50 | 5175.69 ± 50.68 | 50228.35 ± 99.94 |
| $\bar{t}t \rightarrow bWcH$ | 4.43 ± 0.17 | 62.33 ± 0.61 | 49.57 ± 0.55 | 96.13 ± 0.91 |
| $cg \rightarrow tH$ | 0.27 ± 0.01 | 4.78 ± 0.06 | 1.30 ± 0.03 | 5.26 ± 0.07 |
| tcH merged signal | 4.70 ± 0.17 | 67.11 ± 0.62 | 50.87 ± 0.55 | 101.39 ± 0.91 |
| $\bar{t}t \rightarrow bWuH$ | 5.44 ± 0.20 | 64.76 ± 0.63 | 51.94 ± 0.56 | 98.73 ± 0.90 |
| $ug \rightarrow tH$ | 1.48 ± 0.08 | 22.39 ± 0.29 | 7.09 ± 0.16 | 26.96 ± 0.38 |
| tuH merged signal | 6.92 ± 0.21 | 87.15 ± 0.69 | 59.04 ± 0.58 | 125.69 ± 0.98 |

|  | TTH $\tau_{\text{lep}}\tau_{\text{had}}$ ss | TTH $\tau_{\text{lep}}\tau_{\text{had}}$ os | $l\tau_{\text{had}}\tau_{\text{had}}$ 2b ss | $l\tau_{\text{had}}\tau_{\text{had}}$ 2b os |
|---|---|---|---|---|
| data | 5783.00 ± 76.05 | 36026.00 ± 189.81 | 114.00 ± 10.68 | 151.00 ± 12.29 |
| background | 5731.98 ± 34.13 | 36049.34 ± 71.95 | 125.35 ± 3.93 | 128.60 ± 3.98 |
| $\bar{t}t \rightarrow bWcH$ | 40.99 ± 0.50 | 124.40 ± 1.12 | 0.35 ± 0.05 | 5.31 ± 0.18 |
| $cg \rightarrow tH$ | 0.69 ± 0.02 | 4.18 ± 0.07 | 0.01 ± 0.00 | 0.13 ± 0.01 |
| tcH merged signal | 41.69 ± 0.50 | 128.58 ± 1.12 | 0.36 ± 0.05 | 5.44 ± 0.18 |
| $\bar{t}t \rightarrow bWuH$ | 44.39 ± 0.52 | 130.33 ± 1.11 | 0.06 ± 0.02 | 1.28 ± 0.09 |
| $ug \rightarrow tH$ | 4.31 ± 0.14 | 23.43 ± 0.38 | 0.02 ± 0.01 | 0.36 ± 0.04 |
| tuH merged signal | 48.69 ± 0.54 | 153.75 ± 1.17 | 0.09 ± 0.02 | 1.64 ± 0.10 |

|  | STH $\tau_{\text{lep}}\tau_{\text{had}}$ 2b ss | STH $\tau_{\text{lep}}\tau_{\text{had}}$ 2b os | TTH $\tau_{\text{lep}}\tau_{\text{had}}$ 2b ss | TTH $\tau_{\text{lep}}\tau_{\text{had}}$ 2b os |
|---|---|---|---|---|
| data | 1872.00 ± 43.27 | 19549.00 ± 139.82 | 1783.00 ± 42.23 | 11708.00 ± 108.20 |
| background | 1845.32 ± 15.44 | 19500.03 ± 49.14 | 1748.95 ± 14.99 | 11705.94 ± 37.76 |
| $\bar{t}t \rightarrow bWcH$ | 4.21 ± 0.16 | 10.37 ± 0.32 | 3.15 ± 0.14 | 10.21 ± 0.32 |
| $cg \rightarrow tH$ | 0.05 ± 0.01 | 0.28 ± 0.02 | 0.04 ± 0.01 | 0.16 ± 0.01 |
| tcH merged signal | 4.26 ± 0.16 | 10.64 ± 0.32 | 3.19 ± 0.14 | 10.38 ± 0.32 |
| $\bar{t}t \rightarrow bWuH$ | 1.95 ± 0.11 | 4.96 ± 0.21 | 1.69 ± 0.10 | 5.49 ± 0.23 |
| $ug \rightarrow tH$ | 0.26 ± 0.03 | 1.22 ± 0.08 | 0.17 ± 0.03 | 0.87 ± 0.08 |
| tuH merged signal | 2.21 ± 0.11 | 6.18 ± 0.22 | 1.86 ± 0.10 | 6.36 ± 0.24 |

Table 24: The sample and data yield before the fit.

|  | $2lSS\tau_{\text{had}}$ os | $2lSS\tau_{\text{had}}$ os antiiso | $2lSS\tau_{\text{had}}$ os antiisolead |
|---|---|---|---|
| data | 23.00 ± 4.80 | 66.00 ± 8.12 | 19.00 ± 4.36 |
| background | 22.56 ± 1.15 | 67.86 ± 2.90 | 21.92 ± 1.68 |
| $\bar{t}t \rightarrow bWcH$ | 8.66 ± 0.22 | 2.17 ± 0.11 | 0.81 ± 0.07 |
| $cg \rightarrow tH$ | 0.61 ± 0.02 | 0.15 ± 0.01 | 0.04 ± 0.01 |
| tcH merged signal | 9.28 ± 0.23 | 2.32 ± 0.11 | 0.86 ± 0.07 |
| $\bar{t}t \rightarrow bWuH$ | 8.72 ± 0.23 | 2.34 ± 0.12 | 0.81 ± 0.07 |
| $ug \rightarrow tH$ | 3.02 ± 0.11 | 0.77 ± 0.05 | 0.27 ± 0.03 |
| tuH merged signal | 11.74 ± 0.25 | 3.11 ± 0.13 | 1.07 ± 0.08 |

Table 25: The stat. only significance of the signal in each regions with the benchmark $\mu$ value.
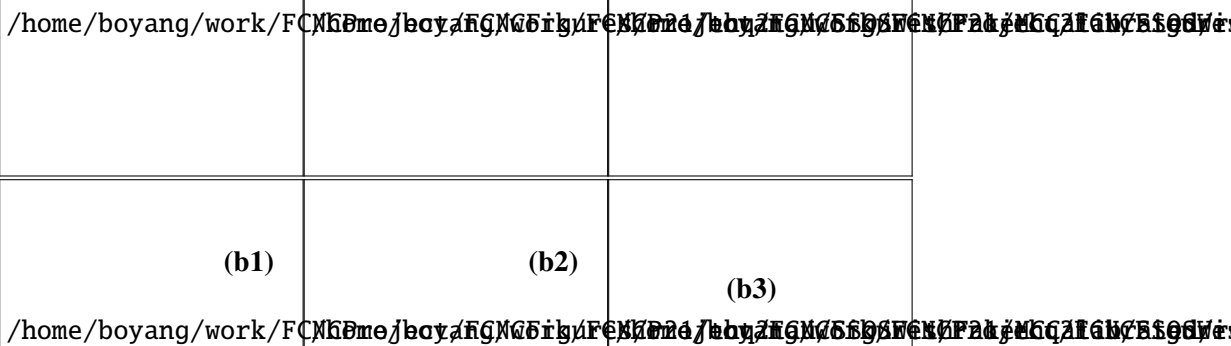
| | $l\tau_{\text{had}}\tau_{\text{had}}$ ss | $l\tau_{\text{had}}\tau_{\text{had}}$ os | STH $\tau_{\text{lep}}\tau_{\text{had}}$ ss | STH $\tau_{\text{lep}}\tau_{\text{had}}$ os |
|---|---|---|---|---|
| $\bar{t}t \to bWcH$ | 0.26 | 5.91 | 0.81 | 0.86 |
| $cg \to tH$ | 0.02 | 0.56 | 0.02 | 0.09 |
| tcH merged signal | 0.27 | 6.31 | 0.83 | 0.94 |
| $\bar{t}t \to bWuH$ | 0.32 | 6.29 | 0.86 | 0.85 |
| $ug \to tH$ | 0.09 | 2.40 | 0.12 | 0.56 |
| tuH merged signal | 0.40 | 8.10 | 0.98 | 1.37 |

| | TTH $\tau_{\text{lep}}\tau_{\text{had}}$ ss | TTH $\tau_{\text{lep}}\tau_{\text{had}}$ os | $l\tau_{\text{had}}\tau_{\text{had}}$ 2b ss | $l\tau_{\text{had}}\tau_{\text{had}}$ 2b os |
|---|---|---|---|---|
| $\bar{t}t \to bWcH$ | 0.59 | 1.94 | 0.04 | 1.01 |
| $cg \to tH$ | 0.01 | 0.09 | 0.00 | 0.02 |
| tcH merged signal | 0.60 | 2.02 | 0.04 | 1.03 |
| $\bar{t}t \to bWuH$ | 0.65 | 2.03 | 0.01 | 0.26 |
| $ug \to tH$ | 0.07 | 0.48 | 0.00 | 0.07 |
| tuH merged signal | 0.72 | 2.50 | 0.01 | 0.32 |

| | STH $\tau_{\text{lep}}\tau_{\text{had}}$ 2b ss | STH $\tau_{\text{lep}}\tau_{\text{had}}$ 2b os | TTH $\tau_{\text{lep}}\tau_{\text{had}}$ 2b ss | TTH $\tau_{\text{lep}}\tau_{\text{had}}$ 2b os |
|---|---|---|---|---|
| $\bar{t}t \to bWcH$ | 0.13 | 0.20 | 0.09 | 0.28 |
| $cg \to tH$ | 0.00 | 0.01 | 0.00 | 0.01 |
| tcH merged signal | 0.13 | 0.21 | 0.09 | 0.28 |
| $\bar{t}t \to bWuH$ | 0.06 | 0.09 | 0.05 | 0.14 |
| $ug \to tH$ | 0.01 | 0.05 | 0.01 | 0.03 |
| tuH merged signal | 0.07 | 0.13 | 0.05 | 0.17 |

Table 26: The stat. only significance of the signal in each regions with the benchmark $\mu$ value.

| | $2lSS\tau_{\text{had}}$ os | $2lSS\tau_{\text{had}}$ os antiiso | $2lSS\tau_{\text{had}}$ os antiisolead |
|---|---|---|---|
| $\bar{t}t \to bWcH$ | 1.75 | 0.27 | 0.20 |
| $cg \to tH$ | 0.23 | 0.04 | 0.04 |
| tcH merged signal | 1.87 | 0.29 | 0.22 |
| $\bar{t}t \to bWuH$ | 1.93 | 0.36 | 0.28 |
| $ug \to tH$ | 1.09 | 0.20 | 0.15 |
| tuH merged signal | 2.76 | 0.53 | 0.41 |

(a1)

/home/boyang/work/FCNCMoEme/boyang/work/FCNCMoEme/boyang/work/FCNCMoEme/boyang/work/FCNCMoEme/boyang/work/FCNCMoEme/boyang/work/FCNCMoEme

(a2)

(a3)

(b1)

/home/boyang/work/FCNCMoEme/boyang/work/FCNCMoEme/boyang/work/FCNCMoEme/boyang/work/FCNCMoEme/boyang/work/FCNCMoEme/boyang/work/FCNCMoEme

(b2)

(b3)



Figure 13: The BDT input distributions for the background and merged signal in the STH $\tau_{\text{had}}\tau_{\text{had}}$ (a1-3), TTH $\tau_{\text{had}}\tau_{\text{had}}$ (b1-3), $l\tau_{\text{had}}\tau_{\text{had}}$ (c1-3) channels.
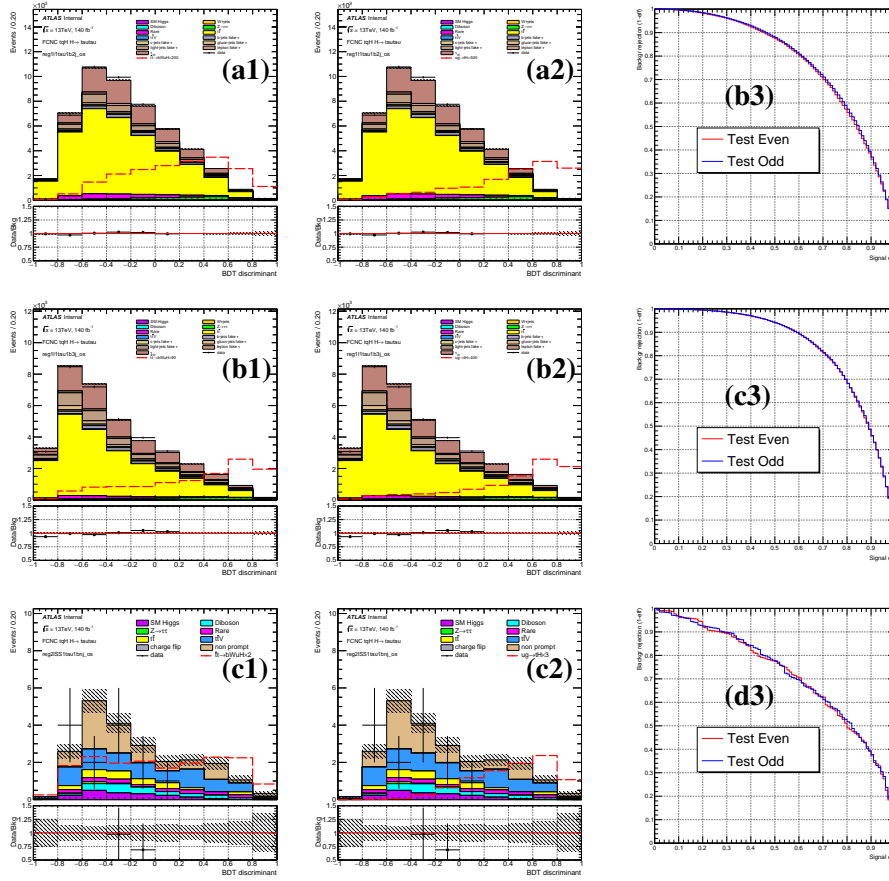
Figure 14: The BDT input distributions for the background and merged signal in the STH $\tau_{\text{lep}}\tau_{\text{had}}$ (a1-3), TTH $\tau_{\text{lep}}\tau_{\text{had}}$ (b1-3), $2lSS\tau_{\text{had}}$ (c1-3) channels.

**(a1)**

/home/boyang/work/FCNChome/boyang/work/FCNChome/boyang/work/FCNChome/boyang/work/FCNChome/boyang/work/FCNC

**(a2)**

**(a3)**

**(b1)**

**(b2)**

**(b3)**

/home/boyang/work/FCNChome/boyang/work/FCNChome/boyang/work/FCNChome/boyang/work/FCNChome/boyang/work/FCNC

Figure 15: The BDT output distributions for the background and TT signal (a1, b1, c1), background and ST signal (a2, b2, c2) and ROC curves (a3, b3, c3) in the STH $\tau_{had}\tau_{had}$ (a1-3), TTH $\tau_{had}\tau_{had}$ (b1-3), $l\tau_{had}\tau_{had}$ (c1-3) channels.

Figure 16: The BDT output distributions for the background and TT signal (a1, b1, c1), background and ST signal (a2, b2, c2) and ROC curves (a3, b3, c3) in the STH $\tau_{\text{lep}}\tau_{\text{had}}$ (a1-3), TTH $\tau_{\text{lep}}\tau_{\text{had}}$ (b1-3), $2lSS\tau_{\text{had}}$ (c1-3) channels.

## 10 Systematic uncertainties

The signal efficiency and the background estimations are affected by uncertainties associated with the detector simulation, the signal modelling and the data-driven background determination. In the combined fit, these uncertainties are called Nuisance Parameters (NP), as opposed to the parameter of interest, the signal strength, which is a scaling factor applied on the total signal events.

Any systematic effect on the the overall normalisation or shape of the final BDT distribution in the signal region is considered. In TRExFitter [**TRExFitter**], the NP pruning is applied, which means that NPs whose impact are less than a certain threshold are discarded. The lower thresholds to remove a shape systematic and a normalisation systematic from the fit are both 1% in the fit.

Table **??** gives the QCD fake estimation for $\tau_{\text{had}}\tau_{\text{had}}$ channel in 8.4 and six fake normalization factor NPs for fake method mentioned in 8.3. The lists of systematic NPs that survive the pruning are in Tab. **??** and **??**, and their meanings are given below. All the NPs in Tab. **??** and the fakeSF* in **??** are fully correlated in all signal regions.

## 10.1 Luminosity

The integrated luminosity measurement has an uncertainty of 1.7% for the combined Run-2 data, and it is applied to all simulated event samples.

## 10.2 Detector-related uncertainties

Uncertainties related to the detector are included for the signal and backgrounds that are estimated using simulation. These uncertainties are also taken into account for the simulated events that enter the data-driven background estimations. All instrumental systematic uncertainties arising from the reconstruction, identification and energy scale of electrons, muons, ($b$-)jets and the soft term of the $E_{\text{T}}^{\text{miss}}$ measurement are considered. The effect of the energy scale uncertainties on the objects is propagated to the $E_{\text{T}}^{\text{miss}}$ calculation. These systematics include uncertainty associated with:

- The electron and muon trigger, reconstruction, identification and isolation efficiencies. These are estimated with the tag-and-probe method on the $Z \rightarrow ll$, $J/\psi \rightarrow ll$ and $W \rightarrow l\nu$ events [**lep_sys**].

- Electron and muon momentum scales. They are estimated from the early 13 TeV $Z \rightarrow ll$ events.

- Jet energy scale (JES) and resolution (JER). The JES uncertainty is estimated by varying the jet energies according to the uncertainties derived from simulation and in-situ calibration measurements using a model with a reduced set of 38 orthogonal NPs [**jet_sys**] which has up to 30% correlation losses, which are assumed to be uncorrelated, and the induced changes can be added in quadrature. The individual scale variations on the jets are parameterised in $p_T$ and $\eta$. The total JES uncertianty is below 5% for most jets and below 1% for central jets with pT between 300 GeV and 2 TeV. The difference between the JER in data and MC is represented by one NP. It is applied on the MC by smearing the jet $p_T$ within the prescribed uncertainty. JVT is applied in the analysis to select jets from hard-scattered vertices. It was found that different MC generators (and different fragmentation models) lead to efficiency differences of up to 1%, and the uncertainty on the efficiency measurement was found to be around 0.5%. Two NPs are assigned for the JVT efficiency, one for the central and the other for the forward jets.

- Calibration of the $E_T^{miss}$. The uncertainties on $E_T^{miss}$ due to systematic shifts in the corrections for leptons and jets are accounted for in a fully correlated way in their evaluation for those physics objects, and are therefore not considered independently here. The systematic uncertainty assigned to the track-based soft term used in the $E_T^{miss}$ definition quantifies the resolution and scale of the soft term measurement by using the balance between hard and soft contributions in $Z \rightarrow \mu\mu$ events. The uncertainties are studied using the differences between Monte Carlo generators, using Powheg+Pythia8 as the nominal generator [**met_sys**]. One NP is assigned for the soft-track scale, and two NPs for the soft-track resolution.

- Jet flavour tagging systematics. The uncertainties on the $b$-tagging are assessed independently for $b$, $c$ and light-flavour quark jets, with extrapolation factors [**btag_sys1**]. The efficiencies and mis-tag rates are measured in data using the methods described in [**btag_sys2**]-[**btag_sys3**] with the 2015, 2016 and 2017 data set. There are 19 NPs assigned for the flavour tagging systematics (so-called "Loose" reduced set, with 5 NPs for light flavor, 4 for $c$, 9 for $b$, and 1 for extrapolation).

- Pileup. The uncertainty on the pileup reweighting is evaluated by varying the pileup scale factors by $1\sigma$ based on the reweighting of the average interactions per bunch crossing. However, this uncertainty is highly correlated with the luminosity uncertainty and may be an overestimate.

- Tau object systematics. These include the $\tau_{had}$ reconstruction, identification and trigger efficiencies, the efficiency for tau-electron overlap removal of true $\tau_{had}$, the one for tau-electron overlap removal of true electrons faking $\tau_{had}$, and the one for a "medium" BDT electron rejection. There are also three NPs that cover the tau energy scale (TES) systematics due to the modeling of the detector geometry (`TAU_TES_DETECTOR`), the measurement in the tag-and-probe analysis (`TAU_TES_INSITU`) and the `Geant4` shower model (`TAU_TES_MODEL`). The systematics are based on detailed MC variation study, as well as the Run-2 $Z \rightarrow \tau\tau$ data for insitu calibrations of the tau TES and trigger efficiencies, as documented in [**tau_sys1**] and the dedicated software tools [**tau_sys2**] recommended by the Tau CP Woking Group [**TauCP**].

## 10.3  Uncertainties on fake background estimations

Systematic uncertainties resulting from the data-driven background estimation and usage of SS events as described in Sec. 8. They are named `fakeSF*prong*Ptbin` and `norm_factor_hh` in Tab. **??**.

## 10.4  Theoretical uncertainties on the background

Theoretical uncertainties have been applied to the MC background in this analysis. The NNPDF3.0 systematic set (which has 100 variations) is used to get the variation envelope around the nominal PDF, and the renormalization and factorization scales are varied by a factor of 0.5 and 2.0 around the nominal values. There are eight such variations. In the final BDT distributions, the largest variations of the eight per bin are taken.

The default $t\bar{t}$ sample is generated with Powheg. A separate full-sim $t\bar{t}$ sample generated with Sherpa (0 and 1-jet at NLO, and $\geq 2$ jets at LO) is compared with the Powheg sample, and the difference in final results is treated as the hard scattering systematics [**ttbarSys**].

The default $t\bar{t}$ MC events are showered with Pythia8. A separate sample showered with Herwig7 is compared with the Pythia8 sample, and the difference is treated as fragmentation and hadronization systematics [**ttbarSys**]. These two samples are both generated with ATLFAST-II [**AFII**], and their difference is then applied to the default full-simulation $t\bar{t}$ sample.

The Powheg+Pythia8 $t\bar{t}$ MC is also generated with different shower radiations (initial and final-state radiation modelling). For a sample with increased radiation, the factorisation and renormalization scales are scaled by 0.5 with respect to their nominal values, the `hdamp` parameter (which controls the amount of radiation produced by the parton shower in `POWHEG-BOX v2`) is set to $3m_{\text{top}}$ and the `A14var3cUp` tune is used. Conversely, for a sample with decreased radiation, the two scales are scaled by 2 with respect to their nominal values, the `hdamp` is kept at the nominal value of $1.5m_{\text{top}}$ and the `A14var3cDown` tune is used [**ttbarSys**].

Uncertainty affecting the normalisation of the $V$+jets background is estimated to be about 30% according to the study done in the FCNC $H \rightarrow b\bar{b}$ channel [**FCNC_Hbb**]. The uncertainty on the diboson cross section is 5% [**VV_uncert**], on single top +5%/−4% [**WtXsec**][**st_uncert_1**, **st_uncert_2**], on $t\bar{t}V$ 15% [**ttV_uncert_1**, **ttV_uncert_2**], and on $t\bar{t}H$ +10%/−13% [**ttH_uncert**].

## 10.5 Uncertainties on the signal modelling

Since the signal samples share the same production as the $t\bar{t}$ process, the systematics listed above for $t\bar{t}$ also apply to the signal. However, because the systematics variation samples are only generated for the SM decays of $t\bar{t}$, only the integral change of the yields observed for the $t\bar{t}$ background with real taus in the FR is used, and applied on the signal in the same region in a fully correlated way. An additional 1.6% uncertainty on BR($H \rightarrow \tau\tau$) is also assigned [**HiggsBR**].

The fake calibration is also applied to the fake tau part of the signal the same way as the background. The 6 NPs are also applied to the signal and fully correlated with the background.

# 11 Fit model and signal extraction

The parameter of interest in this search is the signal strength of the FCNC interactions, BR($t \rightarrow Hq$) and corresponding production mode cross section. The statistical analysis of the data employs a binned likelihood function constructed as the product of Poisson probability terms, in bins of the BDT output.

To take into account the systematic uncertianties associated with the MC estimation from different sources for both the signal and background samples, the fit model incorporates these systematics as extra Gaussian or Log-Normal constraint terms multiplied with the combined likelihood. The fitted central values and errors of the systematics parameters, or NPs, are expected to follow a normal distribution centered around 0 with unit width, when the Asimov data is used. The fit model construction is obtained with the `RooFit` and `RooStats` software, and the model configuration and persistence files (as input to `RooStats`) are produced by `TRExFitter` [**TRExFitter**], which is a software package interface with `HistFactory`. The `TRExFitter` includes additional features such as histogram smoothing, NP pruning and error symmetrization before the fits.

The correlated bin-by-bin histogram variation corresponds to the up and down variation of each NP. The independent bin-by-bin fluctuations in the combined MC templates are also treated as NPs. They are incorporated in the model as extra Poisson constraint terms, and are expected to have a fitted value of 1 and a fitted error reflecting the relative statistical error in each particular bin. There is one parameter if interest (POI) freely floating in the fit without any constraints, namely, the signal strength $\mu$ (`SigXsecOverSM`) which is a multiplicative factor on a presumed branching ratio of BR($t \rightarrow Hq$)=1% in this analysis. The errors associated with the different systematics will be properly propogated to the fitted error of $\mu$ in a simultaneous fit of multiple regions via a profiled likelihood scan by the minimization program `MINUIT`.

The one-sided NPs in the analysis, namely, `fakeSFXprongXPtbin`, `ttbar fragmentation`, `ttbar hard scattering`, `JET_BJES_Response`, `JET_JER_DataVsMC_MC16`, `JET_SingleParticle_HighPt`, `JET_TILECORR_Uncertainty`, `MET_SoftTrk_ResoPara`, `MET_SoftTrk_ResoPerp` are symmetrized. This is done manually on the MC components of the background. By default, all the kinematic NPs (shape NPs due to, e.g., energy scales) are smoothed using the default smoothing parameters in `TRExFitter`. This helps removing the artificial NP constraints due to statistical fluctuations in the systematic variations, and makes the fit well behaved. The NPs pull distributions before the smoothing for each SR are given in App. **??**.

Figure 20 shows the ranking of the 25 top NPs along with their pull distributions, produced also with TRExFitter. The highest ranked NP is defined to have the largest impact on $\mu$. The impact is evalated by varying the NP under consideration by one $\sigma$ (either pre or post-fit error) up and down, and afterwards looking at the relative change in $\mu$ under the conditional fit where the NP under consideration is fixed to its varied new value. Figure **??** shows the pull distributions of all NPs in asimov fit. Normalization and

734  shape systematics whose impact is less than 1% are removed from the fit. The list of removed NPs are
735  given in App. **??**.

736  The NP ranking and constraints can be qualitatively understood from the variations of the BDT distributions
737  due to the relevant NPs. Figures **??-??** show the systematic variations due to the top ranked NPs.

738  Figure 21 shows the correlation matrix for diffrent NPs. Except for self-correlations, and the correlations
739  between the normalization factors (including POI) and the others, all the NPs have relatively small
740  correlations with each other, which justifies the fit models for independent systematics.
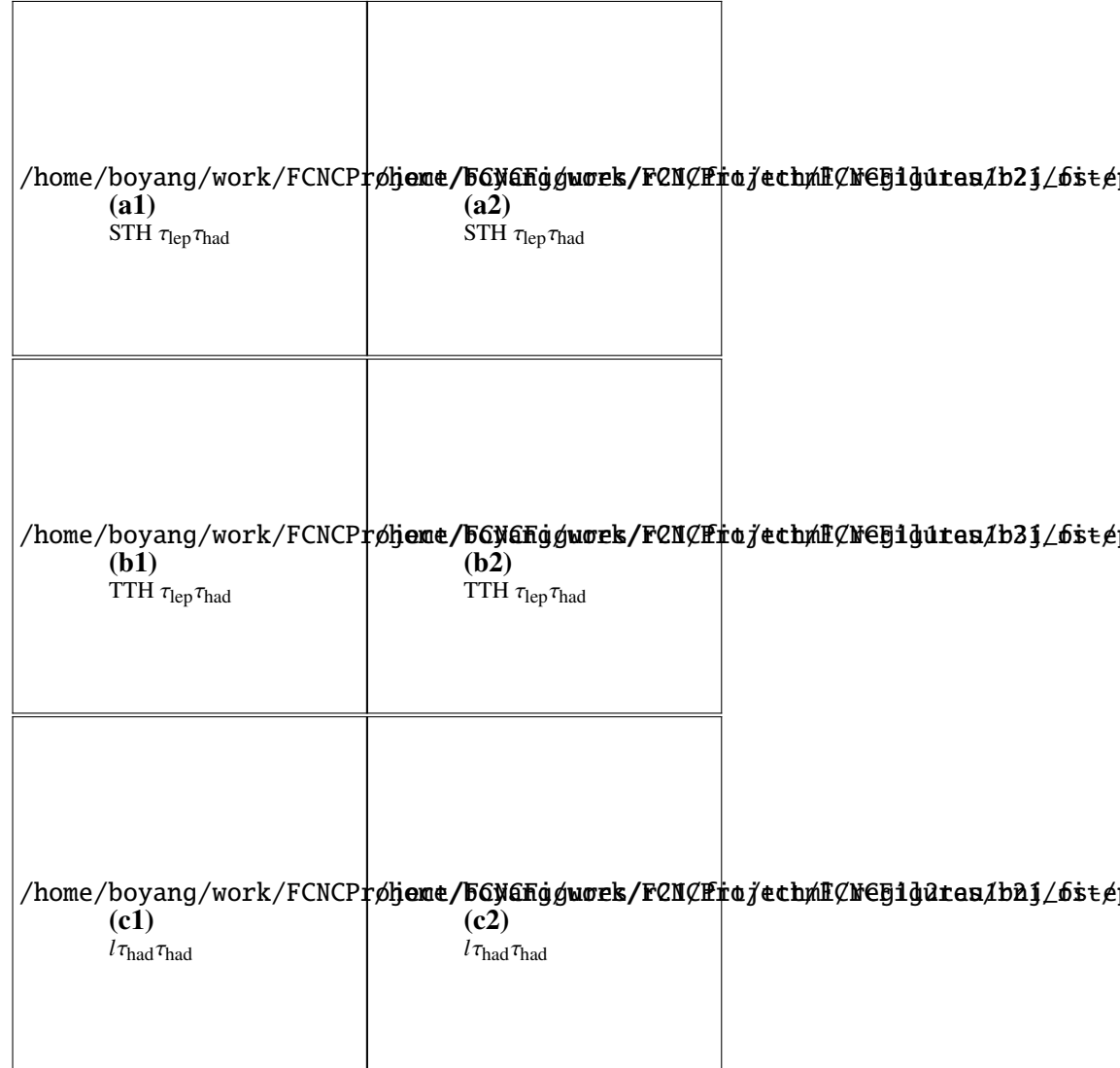


Figure 17: The asimov prefit (left) and postfit (right) BDT distributions in the STH $\tau_{\mathrm{lep}}\tau_{\mathrm{had}}$ (a1-2) and TTH $\tau_{\mathrm{lep}}\tau_{\mathrm{had}}$ (b1-2), $l\tau_{\mathrm{had}}\tau_{\mathrm{had}}$ (c1-2)

/home/boyang/work/FCNCProject/home/boyang/work/FCNCProject/FCNCFigures/fits/
**(a1)**
TTH $\tau_{\text{had}}\tau_{\text{had}}$

/home/boyang/work/FCNCProject/home/boyang/work/FCNCProject/FCNCFigures/fits/
**(a2)**
TTH $\tau_{\text{had}}\tau_{\text{had}}$

/home/boyang/work/FCNCProject/home/boyang/work/FCNCProject/FCNCFigures/fits/
**(b1)**
STH $\tau_{\text{had}}\tau_{\text{had}}$

/home/boyang/work/FCNCProject/home/boyang/work/FCNCProject/FCNCFigures/fits/
**(b2)**
STH $\tau_{\text{had}}\tau_{\text{had}}$

Figure 18: The asimov prefit (left) and postfit (right) BDT distributions in the TTH $\tau_{\text{had}}\tau_{\text{had}}$ (a1-2) and STH $\tau_{\text{had}}\tau_{\text{had}}$ (b1-2)

/home/boyang/work/FCNCProject/FCNCFigures/home/boyang/work/FCNCProject/FCNCFigures/or2d/fit/
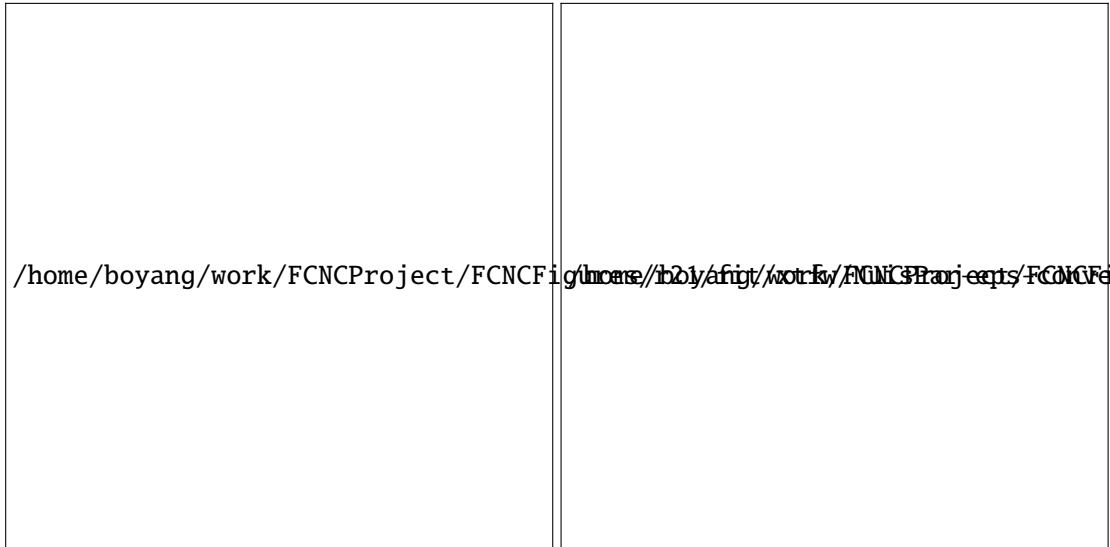
Figure 19: The asimov fit pull distributions of different NPs for $\tau_{\text{had}}\tau_{\text{had}}$ channels (left) combined and lepton channels combined (right).

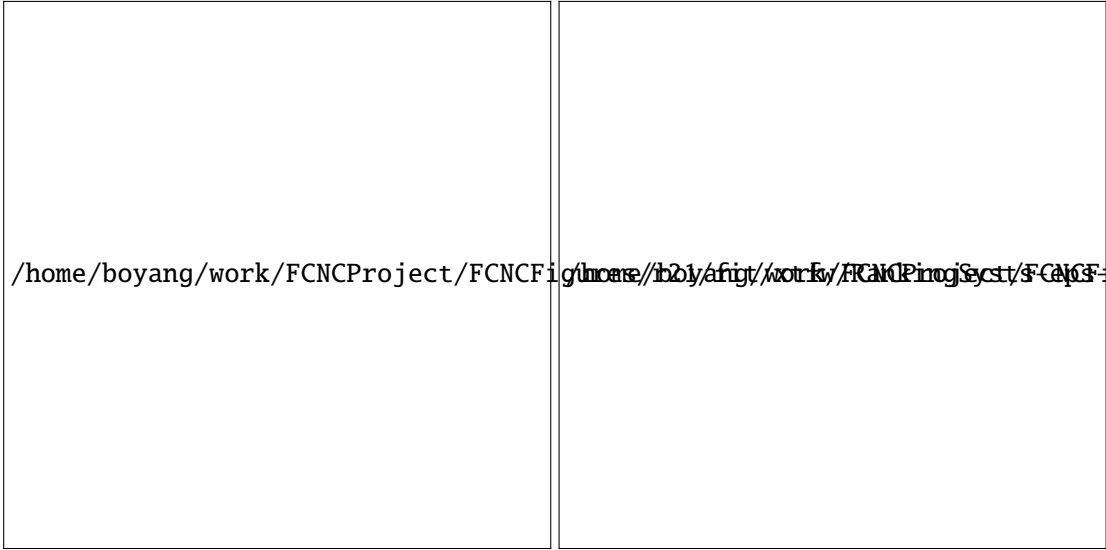/home/boyang/work/FCNCProject/FCNCFig/home/b2y/afig/work/FCNCProg/syst/FCNC-iconves/r2d-tfoi.tp/

Figure 20: The asimov fit ranking of the top 25 NPs for $\tau_{had}\tau_{had}$ channels (left) combined and lepton channels combined (right). The scale of the relative impact on $\mu$ (the pull) of the NPs is shown on the top (bottom) axis.
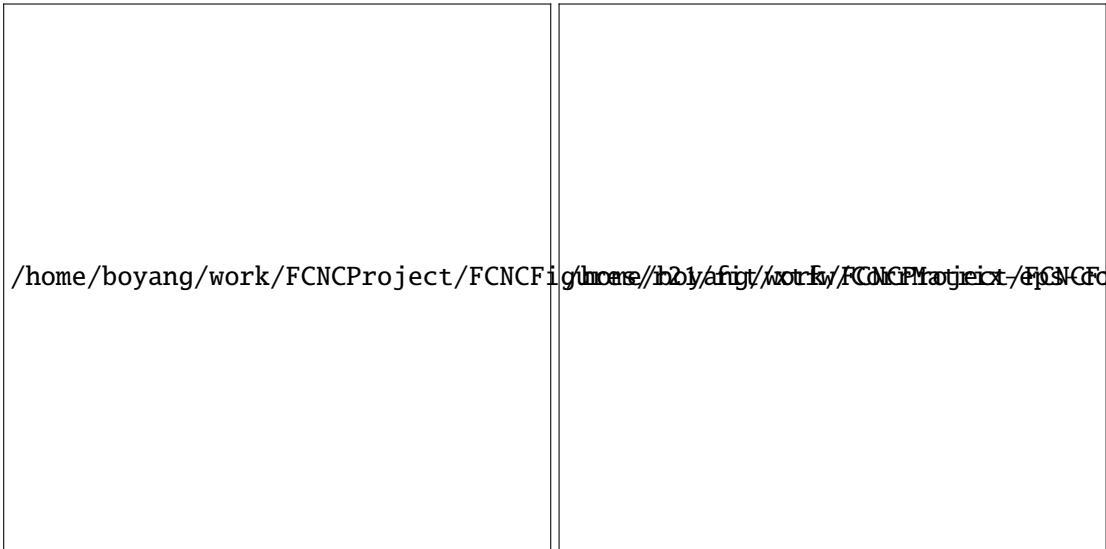
/home/boyang/work/FCNCProject/FCNCFig/home/b2y/afig/work/FCNCProject/FCNC-Figuenets/d-2to/.fidtf/

Figure 21: The asimov fit correlation matrix (%) of different NPs, with a threshold of 20% for $\tau_{had}\tau_{had}$ channels (left) combined and lepton channels combined (right).

## 12 Results

The significance of any small observed excess in data is evaluated by quoting the $p$-values to quantify the level of consistency of the data with the BR=0 hypothesis. The asymptotic approximation in [**CCGV**] is used. The test statistic used for the exclusion limits derivation is the $\tilde{q}_\mu$ test statistic and for the $p$-values the $q_0$ test statistic[6] [**CCGV**].

The 95% CL upper limits on tqH interaction with $\mathrm{BR}(t \to Hq) = 0.2\%$ as reference are given in Tab. 27. The best asimov fit values with S+B hypothesis are given in Tab. **??**

Table 27: The expected 95% CL exclusion upper limits on $\mathrm{BR}(t \to Hc)$ and $\mathrm{BR}(t \to Hu)$ (0.2%) with the Asimov (B-only).

|  | $tcH$ | $tuH$ |
|---|---|---|
| $\tau_{\mathrm{had}}\tau_{\mathrm{had}}$ | $0.80^{+0.41}_{-0.22}$ | $0.64^{+0.33}_{-0.18}$ |
| leptonic channels | $0.77^{+0.33}_{-0.21}$ | $0.60^{+0.26}_{-0.17}$ |

Table 28: The best asimov fit values with S+B hypothesis.

|  | $tcH$ | $tuH$ |
|---|---|---|
| $\tau_{\mathrm{had}}\tau_{\mathrm{had}}$ | $1.00^{+0.23+0.51}_{-0.22-0.38}$ | $1.00^{+0.18+0.44}_{-0.18-0.33}$ |
| leptonic channels | $1.00^{+0.56+X.XX}_{-0.54-X.XX}$ | $1.00^{+0.47+X.XX}_{-0.46-X.XX}$ |

The search for the FCNC decay $t \to Hq, H \to \tau\tau$ with the ATLAS detector at the LHC using 13 TeV data was presented in this note. The best-fit values for $\mathrm{BR}(t \to Hc)$ and $\mathrm{BR}(t \to Hu)$ are found to be $-X.XX^{+X.XX}_{-X.XX}\%$ and $-X.XX^{+X.XX}_{-X.XX}\%$ respectively, based on 140 fb$^{-1}$ of data collected from 2015 to 2018. The observed (expected) 95% CL upper limits on $\mathrm{BR}(t \to Hc)$ and $\mathrm{BR}(t \to Hu)$ are found to be $X.XX\%$ ($X.XX^{+X.XX}_{-X.XX}\%$) and $X.XX\%$ ($X.XX^{+X.XX}_{-X.XX}\%$), respectively.

---

[6] The definition of the test statistics used in this search is the following:

$$\tilde{q}_\mu = \begin{cases} -2\ln(\mathcal{L}(\mu,\hat{\hat{\theta}})/\mathcal{L}(0,\hat{\hat{\theta}})) & \text{if } \hat{\mu} < 0 \\ -2\ln(\mathcal{L}(\mu,\hat{\hat{\theta}})/\mathcal{L}(\hat{\mu},\hat{\theta})) & \text{if } 0 \leq \hat{\mu} \leq \mu \\ 0 & \text{if } \hat{\mu} > \mu \end{cases}$$

and

$$q_0 = \begin{cases} -2\ln(\mathcal{L}(0,\hat{\hat{\theta}})/\mathcal{L}(\hat{\mu},\hat{\theta})) & \text{if } \hat{\mu} \geq 0 \\ 0 & \text{if } \hat{\mu} < 0 \end{cases}$$

where $\mathcal{L}(\mu,\theta)$ denotes the binned likelihood function, $\mu$ is the parameter of interest (i.e. the signal strength parameter), and $\theta$ denotes the nuisance parameters. The pair $(\hat{\mu},\hat{\theta})$ corresponds to the global maximum of the likelihood, whereas $(x,\hat{\hat{\theta}})$ corresponds to a conditional maximum in which $\mu$ is fixed to a given value $x$.

# 753 Appendix

# List of contributions

- Boyang Li: main analyser, signal generation; ntuple production; fake tau estimation; BDT analysis; systematics; fit; support note.

- Weiming Yao: main analyser, `ttHML` ntuple skimming and support; fake tau estimation; BDT analysis; cross check; support note.

- MingMing Xia: main analyser, `xTauFramework` n-tuple production; production validation.

- Xin Chen: Supervisor of Boyang Li and MingMing Xia